University of Windsor

Scholarship at UWindsor

2005

Mesoporous tantalum oxide catalysts for nitrogen fixation.

Chaoyang Yue
University of Windsor

Follow this and additional works at: https://scholar.uwindsor.ca/etd

Recommended Citation

Yue, Chaoyang, "Mesoporous tantalum oxide catalysts for nitrogen fixation." (2005). *Electronic Theses and Dissertations*. 2708.
https://scholar.uwindsor.ca/etd/2708

This online database contains the full-text of PhD dissertations and Masters' theses of University of Windsor students from 1954 forward. These documents are made available for personal study and research purposes only, in accordance with the Canadian Copyright Act and the Creative Commons license—CC BY-NC-ND (Attribution, Non-Commercial, No Derivative Works). Under this license, works must always be attributed to the copyright holder (original author), cannot be used for any commercial purposes, and may not be altered. Any other use would require the permission of the copyright holder. Students may inquire about withdrawing their dissertation and/or thesis from this database. For additional inquiries, please contact the repository administrator via email (scholarship@uwindsor.ca) or by telephone at 519-253-3000ext. 3208.

Mesoporous Tantalum Oxide Catalysts for Nitrogen Fixation

by

Chaoyang Yue

A Thesis
Submitted to the Faculty of Graduate Studies and Research
through the Department of Chemistry and Biochemistry
in Partial Fulfillment of the Requirements for
the Degree of Master of Science at the
University of Windsor

Windsor, Ontario, Canada
2005

© 2005 Chaoyang Yue

Library and
Archives Canada

Published Heritage
Branch

395 Wellington Street
Ottawa ON K1A 0N4
Canada

Bibliothèque et
Archives Canada

Direction du
Patrimoine de l'édition

395, rue Wellington
Ottawa ON K1A 0N4
Canada

Your file Votre référence
ISBN: 0-494-09826-0
Our file Notre référence
ISBN: 0-494-09826-0

NOTICE:
The author has granted a non-exclusive license allowing Library and Archives Canada to reproduce, publish, archive, preserve, conserve, communicate to the public by telecommunication or on the Internet, loan, distribute and sell theses worldwide, for commercial or non-commercial purposes, in microform, paper, electronic and/or any other formats.

The author retains copyright ownership and moral rights in this thesis. Neither the thesis nor substantial extracts from it may be printed or otherwise reproduced without the author's permission.

AVIS:
L'auteur a accordé une licence non exclusive permettant à la Bibliothèque et Archives Canada de reproduire, publier, archiver, sauvegarder, conserver, transmettre au public par télécommunication ou par l'Internet, prêter, distribuer et vendre des thèses partout dans le monde, à des fins commerciales ou autres, sur support microforme, papier, électronique et/ou autres formats.

L'auteur conserve la propriété du droit d'auteur et des droits moraux qui protège cette thèse. Ni la thèse ni des extraits substantiels de celle-ci ne doivent être imprimés ou autrement reproduits sans son autorisation.

In compliance with the Canadian Privacy Act some supporting forms may have been removed from this thesis.

While these forms may be included in the document page count, their removal does not represent any loss of content from the thesis.

Conformément à la loi canadienne sur la protection de la vie privée, quelques formulaires secondaires ont été enlevés de cette thèse.

Bien que ces formulaires aient inclus dans la pagination, il n'y aura aucun contenu manquant.

Canada

1030380

Abstract

A variety of mesoporous tantalum oxide supported catalytic systems were synthesized and investigated for their activities in nitrogen activation, including the Schrauzer-type photocatalytic process and the Haber-Bosch type thermocatalytic process. Mesoporous Ta oxide possesses a high thermal stability, high surface area, tunable wall composition and, most interestingly, variable oxidation states of the transitional metal sites. For this reason it represents a unique support for heterogeneous catalysis. Modification of the surface properties by doping active metal agents and various thermal treatments can further improve the activity. Results obtained in this work showed that for the photocatalytic process pure Ta oxide, with suitable band gap near-UV, exhibited relatively low activity; however, 1 wt% Fe^{3+} doping increased the activity by a factor of 3. For the Haber process, the Ba-Ru-Ta material was the most active system. $Ru_3(CO)_{12}$ proved to be the best precursor for the active Ru metal component, and $Ba(NO_3)_2$ was the best precursor for the BaO promoter. Remarkably, this system shows a very low activation energy of 9.3 kJ/mol as well as a clear involvement of Ta specie(s) during the catalytic reaction. This suggests a different mechanism than that proposed for standard Ru-based Haber synthesis, which uses alumina, silica and magnesia supports, might be functioning. The results in this thesis clearly show the enormous potential of mesoporous transition metal oxides in catalysis, the first porous support materials offering variable oxidation states. All materials in this work were characterized by a combination of techniques including XRD, TEM, nitrogen adsorption, XPS, EDS, and H_2-TDA.

Co-Authorship Statement

This thesis incorporates the outcome of research undertaken in collaboration with Dr. Michel Trudeau as part of a research project under the supervision of Professor David M. Antonelli. The collaboration related to research in TEM and XPS studies is covered in Chapter 2 and Chapter 3 of this thesis.

I certify that, with the above qualification, this thesis, and the research to which it refers, are the product of my own work, and that any ideas or quotations from the work of other people, published or otherwise, are fully acknowledged in accordance with the standard referencing practices of the discipline. I acknowledge the helpful guidance and support of my supervisor, Professor David M. Antonelli.

Acknowledgements

I'm pleased to acknowledge those who have helped with my graduate study, beginning with my supervisor Dr. David M. Antonelli. He is such a wonderful advisor who not only achieved great successes himself, but also is enthusiastic in helping me learn and grow, monitoring my progress and generous about giving credit when it was due. His academic advice and generous financial support have always been highly appreciated.

I'm very grateful to our collaborator Dr. Michel Trudeau, who gave me a lot of help with the analysis of XPS and TEM samples. I'm also grateful to Mr. J. Robinson for his help with running EDS samples.

Many thanks are given to our group members, Dr. Boris Skadtchenko, Dr. Longhui Qiu, Dr. Abdul Seayad, Mr. Xin Hu, Mr. Yuxiang Rao and Mr. Anderei Lezau for their help and advice. Extra thanks are given to Dr. Boris Skadtchenko, his generous help can be seen almost everyday through the time. I also thank, from the bottom of my heart, the faculty and staffs of Department of Chemistry and Biochemistry, University of Windsor, for their support and kind help during the period of my graduate study. The department really impressed me as a sweat, warm big family.

Finally, the continual encouragement and support of my family, my parents and my friends has been a source of strength, which is sincerely appreciated.

Table of Contents

Abstract iii

Co-Authorship Statement iv

Acknowledgements v

List of Figures ix

List of Tables xiii

List of Abbreviations xiv

Chapter 1. Introduction 1

1.1 Importance of Catalysis 1

1.2 Classification of Heterogeneous Catalysts 3

1.2.1 Metal Catalysts 3

1.2.2 Oxide Catalysts 5

1.2.3 Zeolites 6

1.2.4 Sulfide Catalysts 8

1.3 Development History of Mesoporous Materials 8

1.4 Current Status of Mesoporous Transition Metal Oxides as Catalysts 12

1.5 Nitrogen Activation 13

1.5.1 Homogeneous Nitrogen Activation 15

1.5.2 Heterogeneous Nitrogen Activation - Haber-Bosch Process 20

1.5.2.1 Mechanism and Kinetics 21

1.5.2.2 Structure Sensitivity of Fe Catalyst 22

1.5.2.3 Effects of Aluminum Oxide 23

1.5.2.4 Effects of Potassium 23

1.5.3 Ru-based Catalyst - the Second Generation 24

1.6 Nitrogen Activation on Bis-toluene Ti/Nb Reduced Mesostructure Systems 27

Chapter 2. Mesoporous Tantalum Oxide Photocatalysts for Schrauzer-Type Conversion of Dinitrogen to Ammonia 30

2.1 Experimental Section 33

2.1.1 Chemical and Catalyst Preparation 33

2.1.2 Apparatus and Procedure for Photocatalysis 34

2.1.3 Characterization 35

2.14 Stock Reagents for Indophenol Blue Method 35

2.2 Results and Discussion 36

2.2.1 Pure Mesoporous Tantalum Oxide 36

2.2.2 Fe^{3+} Doped Mesoporous Tantalum Oxides 40

2.2.3 Mesoporous Ta oxide Reduced with Bis (toluene) Titanium 43

2.3 Conclusion 45

Chapter 3. Electroactive Mesoporous Tantalum Oxide Catalysts for Nitrogen Activation and Ammonia Synthesis 46

3.1 Experimental Section 47

3.2 Results and Discussion 49

3.3 Conclusion 57

Chapter 4. Support and Promoter Effect of Ru-based Mesorporous Ta Oxide Catalysts for Ammonia Synthesis 58

4.1 Experimental Section 60

4.1.1 Materials and Equipment 60

4.1.2 Synthesis 60

4.2 Results and Discussion 61

4.2.1 Characterization 61

4.2.2 Effect of Reduction Temperature 63

4.2.3 Effect of Different Promoters 66

4.2.3 Effect of Promoter/Ru ratio 70

4.2.4 Effect of Absolute Ru Loading 71

4.2.5 Effect of Ba and Ru Precursor 73

4.3 Conclusion 75

Chapter 5. Conclusion 76

References 83

Vita Auctoris 92

List of Figures

Chapter 1. Introduction

Figure 1. Activation energies and their relationship to an active and selective catalyst. 1

Figure 2. Scheme for the generation of Brønsted and Lewis acid sites in zeolites. 7

Figure 3. A schematic overview of three liquid crystal templating models. 10

Figure 4. Schematic representation of possible synthesis pathway for Nb-TMS1 under a ligand-assisted templating mechanism. 12

Figure 5. Schematic representation of a typical bacterial nitrogen-fixing system. 14

Figure 6. Proposed reactions for dinitrogen cleavage over a three – coordinate molybdenum (III) complex. 16

Figure 7. Reaction of dinulear zirconium complex with H_2 to form a N-H unit and a bridging hydride. 17

Figure 8. Proposed intermediates in the reduction of dinitrogen at a single molybdenum center through the stepwise addition of protons and electrons. 18

Figure 9. Scheme for hydrogenation of dinuclear zirconium complex and cleavage of N_2. 19

Figure 10. Scheme for formation of both side-on and end-on dinitrogen coordination from a dinuclear tantalum complex. 20

Figure 11. Schematic representations of the idealized surface structure of the (111), (211), (100), (210), and (110) orientation of iron single crystals. 22

Figure 12. Schematic representation of deposition of Nb atoms from bis(toluene) niobium to the inner surface of a mesoporous oxide to form a low-valent metallic oxide coating on the internal surface. 28

Chapter 2. Mesoporous Tantalum Oxide Photocatalysts for Schrauzer-Type Conversion of Dinitrogen to Ammonia

Figure 13. Standard curve of absorbance versus concentration for indephenol blue method. 34

Figure 14. X-Ray powder diffraction patterns for (a) mesoporous Ta oxide (S1), b)mesoporous Ta oxide after calcination at 300°C for 3h (S7), and c) 1% Fe^{3+}-doped mesoporous Ta oxide after calcination at 300°C for 3h (S8). 36

Figure 15. Nitrogen adsorption-desorption isotherms for (a) mesoporous Ta oxide (S1), (b)mesoporous Ta oxide after calcination at 300 °C for 3h (S7), and c) 1% Fe^{3+}-doped mesoporous Ta oxide after calcination at 300°C for 3h (S8). 37

Figure 16. TEM of pure mesoporous Ta oxide (S1). 37

Figure 17. XPS spectra of the Ta 4f region for S7 (a) before photocatalytic reaction, and (b) after a 3 h photocatalytic reaction. 39

Figure 18. XPS spectra of the N 1s region for S7 (a) before photocatalytic reaction, and (b) after a 3 h photocatalytic reaction. 39

Figure 19. Comparison experiments on S8 under UV lamp, (a) Helium is the only feeding gas, and (b) a mixture of N_2+H_2O is the feeding gas. 42

Figure 20. Comparison experiments on S5 under UV lamp, (a) Helium is the only feeding gas, and (b) a mixture of N_2+H_2O is the feeding gas. 42

Chapter 3. Electroactive Mesoporous Tantalum Oxide Catalysts for Nitrogen Activation and Ammonia Synthesis

Figure 21. X-ray powder diffraction patterns for (a) mesoporous Ta oxide starting material, (b) parent catalyst Ba-Ru/Ta oxide, (c) catalyst after catalytic run at 175°C, 3h, and (d) catalyst after H_2 regeneration at 350°C, 2h. 49

Figure 22. EDS of 5% Ru-doped mesoporous Ta oxide. 50

Figure 23. Natural log of incremental activity versus time at 350°C of the catalyst from Figure 21b. 51

Figure 24. Arrhenius plot for the catalyst from Figure 21b. 52

Figure 25. XPS spectra of the Ta 4f region for (a) parent catalyst Ba-Ru/Ta oxide, (b) after catalytic run at 175°C, 3h, and (c) catalyst after H_2 regeneration at 350°C, 2h. 54

Figure 26. XPS spectra of the Ru 3p region for (a) parent catalyst Ba-Ru/Ta oxide, (b) after catalytic run at 175°C, 3h, and (c) catalyst after H_2 regeneration at 350°C, 2h. 54

Figure 27. Possible mechanism for ammonia formation on Ru-doped mesoporous Ta oxide materials showing reduced Ta sites in dark blue. 55

Chapter 4. Support and Promoter Effect of Ru-based Mesorporous Ta Oxide Catalysts for Ammonia Synthesis

Figure 28. TEM of 5% Ru-doped mesoporous Ta oxide. 62

Figure 29. Nitrogen adsorption-desorption isotherms for (a) pure mesoporous Ta oxide, (b) catalyst Ba-Ru/Ta(Ru=5wt%, molar ratio Ba/Ru=1) before H_2 activation, and (c) catalyst from (b) after H_2 activation at 350°C for 4h, followed by catalytic run at 175°C. 63

Figure 30. Activity of ammonia synthesis on 5 wt% Ru-Cs/Ta and Ru-Ba/Ta oxides (promoter/Ru=1 mol/mol) as a function of the reduction temperature. The rate was measured at 623K. 64

Figure 31. H_2-DTA of Ru/Ta oxide catalysts promoted with $Ba(NO_3)_2$ for (a) Ba/Ru=1, and (b) Ba/Ru=3. 65

Figure 32. Activity of ammonia synthesis on 5 wt% Ba-Ru/Ta as a function of Ba/Ru mol ratio. ▲: rate was measured at 448K on the catalyst reduced at 623K; ■: rate was measured at 623K on the catalyst reduced at 623K. 70

Figure 33. Activity of ammonia synthesis at 448K (▲) and 623K (■) as a function of Ru loading. 72

List of Tables

Chapter 1. Introduction

Table 1. Examples of heterogeneous catalysis. 2

Table 2. Up to date studies of mesoporous metal oxides in catalysis. 13

Table 3. Reactivity of five Fe crystal faces. 23

Chapter 2. Mesoporous Tantalum Oxide Photocatalysts for Schrauzer-Type Conversion of Dinitrogen to Ammonia

Table 4. Effects of thermal pretreatment and Fe^{3+} doping on photocatalytic activity. 38

Chapter 3. Electroactive Mesoporous Tantalum Oxide Catalysts for Nitrogen Activation and Ammonia Synthesis

Table 5. Activities at different reaction temperatures. 52

Table 6. Surface areas of catalyst from Figure 24 after subsequent steps in the catalytic process. 56

Chapter 4. Support and Promoter Effect of Ru-based Mesorporous Ta Oxide Catalysts for Ammonia Synthesis

Table 7. Promoter effect on the rate of ammonia synthesis over 5 wt% Ru/Ta oxide. 64

Table 8. Effect of Ru and Ba precursor. 74

List of Abbreviations

International Union of Pure and Applied Chemistry	IUPAC
The Family of Silica Based Mesoporous Materials	M41S
Mobil Composition of Matter-41, Hexagonal Mesoporous Phase	MCM-41
Mobil Composition of Matter-48, Cubic Mesoporous Phase	MCM-48
Mobil Composition of Matter-50, Hexagonal Mesoporous Phase	MCM-50
Hexagonally Ordered Mesoporous Niobium Oxide	Nb-TMS1
Hexagonally Ordered Mesoporous Tantalum Oxide	Ta-TMS1
Hexagonally Ordered Mesoporous Titanium Oxide	Ti-TMS1
Liquid Crystal Template	LCT
Ligand Assisted Template	LAT
Tetrahydrofuran	THF
X-ray Diffraction	XRD
X-ray Photoelectron Spectroscopy	XPS
Nuclear Magnetic Resonance	NMR
Ultraviolet	UV
Fourier Transform Infra-Red Spectroscopy	FT-IR
Fourier Transform Raman Spectroscopy	FT-Raman
UV-Vis Diffuse Reflectance Spectroscopy	UV-Vis DRS
Hydrogen Temperature Programmed Reduction	H_2-TPR
Temperature Programmed Desorption	TPD
Hydrogen Differential Thermal Analysis	H_2-DTA

X-ray Absorption Near Edge Structure	XANES
Extended X-ray Absorption Fine Structure	EXAFS
Energy Dispersive X-ray Spectroscopy	EDS
Brunauer, Emmett, Teller	BET
Horvath-Kowazoe	HK
Transmission Electron Microscopy	TEM
Active Carbon	A.C.
Strong Metal-Support Interaction	SMSI
Kellogg Advanced Ammonia Process	KAAP
Hexa-Iso-Propyl-Terphenyl	HIPT
$PhP(SiMe_2CH_2NPh)_2$	NPN
$PhP(CH_2SiMe_2NSiMeCH_2)_2PPh$	P_2N_2

Chapter1. Introduction

1.1 Importance of Catalysis

The word "catalysis" was coined by Berzelius in 1836 [1, 2] to define acceleration of a chemical reaction induced by the presence of material that is chemically unchanged at the end of the reaction. This material, which acts as an active chemical spectator, is a *catalyst*. A catalyst exerts its "catalytic force" by lowering activation barrier,[3] thus speeding up the chemical reaction, but not changing the properties of the equilibrated state (Figure 1).

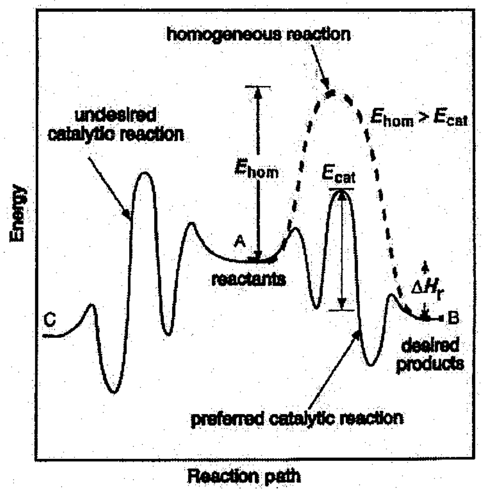
homogeneous reaction
undesired catalytic reaction
$E_{hom} > E_{cat}$
E_{hom}
E_{cat}
A
reactants
C
ΔH_r
B
desired products
preferred catalytic reaction
Energy
Reaction path

Figure 1. Activation energies and their relationship to an active and selective catalyst. E_{hom} - activation barrier for the homogeneous reaction; E_{cat} - activation barrier with use of catalyst; ΔH r, change in enthalpy of reactants compared with product. (Reprinted from Kolasinski, K. W. *Surface Science: Foundations of Catalysis and Nanoscience*, John Wiley & Sons, **2002**)

Heterogeneous catalysis is a catalyzed reaction in which the catalyst is in a different phase from the reactants, for example, liquids and solids, or gases and solids; therefore, the reaction occurs at the interface between these two phases.[4] Heterogeneous catalysis is the foundation of the chemical industry. The successful implementation of heterogeneous catalysis is not only responsible for billions of pounds worth of products required by modern society, but also is essential for the reduction of air and water pollution. "One-third of material gross national product in the U.S. involves a catalytic process somewhere in the production chain" claimed a recent article concerning the economic contribution of catalysis. [5]

However, acceleration of a reaction is not only the crucial factor in catalytic activity; an ideal catalyst should have high activity as well as good selectivity, that is, speeding up one particular reaction, not simply every reaction. In addition to creating desired products, catalysis can also be used to decompose undesirable molecules. Three excellent examples of heterogeneous catalysis are listed in Table 1, because of their particular importance both historically and economically.

Table 1. Examples of heterogeneous catalysis.

Process	Reactants	Product(s)	Catalyst	Key factor
Haber-Bosch process	$H_2 + N_2$	NH_3	Fe	Activity
Fischer-Tropsch chemistry	$H_2 + CO$	Methanol, liquid fuels, hydrocarbons(HCs), oxygenates	Fe, or Co	Selectivity
Three-way catalyst	NO_x, CO, and HC	H_2O, CO_2, N_2	Combo of Pt, Rh, and Pd	Conversion

The Haber-Bosch process is employed to produce vast amount of nitrogen fertilizers which underpin modern agriculture.[6] Since NH_3 is a very thermodynamically stable nitrogen hydride, *selectivity* is not a problem for this catalyst. Therefore, whether or not this catalyst can efficiently break the N≡N bond, thus activating initially inert N_2 with high turnover rate (*activity*), becomes the key to the Haber-Bosch process.

Fischer-Tropsch (F-T) chemistry is the basis of the synthetic fuels industry [7] and has a far-reaching influence on sustainable development of economies that were shut off from crude oil; Fischer-Tropsch chemistry also transforms 'syn gas' into more useful intermediate chemicals. Obviously, selectivity is the most important requirement of F-T catalyst because numerous products are possible, as we see in Table 1, but only a select few are desired for any particular application.

Interest in improving three-way catalytic converters is continuing to rise with increasing automobile use.[8] Unlike Haber-Bosch process and Fischer-Tropsch chemistry, three-way catalysts are responsible for the conversion of noxious exhaust gases to more benign chemicals. As environment becomes a key of the 21st century, more and more strict regulations have been imposed on the release of NOx, CO and CHs in automotive emissions worldwide, which represents a big challenge to catalytic chemistry.

1.2 Classification of Heterogeneous Catalysts

The overwhelming majority of commonly used catalysts can be sorted into four groups: metal, oxide, zeolite, and sulfide. Other types of catalysts of interest, for example halogenation catalysts, because of their thermal instability under normal operation conditions, will not be included in this discussion.

1.2.1 Metal Catalysts

Metal catalysts include bulk metal catalysts and supported metal catalysts. Bulk metal catalysts are much less popular than supported metal catalysts because of their high cost. However, in some cases, bulk metal catalysts can achieve very good selectivity which, otherwise, can't be replicated by their supported analogues.

Silver, when used without a support, represents a very good example of a bulk metal catalyst that promotes selective oxidation reaction from methanol to formaldehyde.[9] Unlike most other metal catalysts, which tend to produce fully oxidized products, silver is able to partially oxidize methanol to formaldehyde at an operative temperature of around 600°C. Elementary steps of methanol oxidation over a silver catalyst are showing below, surface species indicated by (s). The rate-limiting step in the overall reaction is the breaking of a carbon-hydrogen bond (step 1.4). This hydrogen abstraction is carried out by a surface silver atom and is followed by rapid desorption of formaldehyde.

$$\begin{array}{ll}
1/2O_2 \rightarrow O_{(S)} & (1.1) \\
2CH_3OH + 2O_{(S)} \rightarrow 2CH_3O + 2OH_{(S)} & (1.2) \\
2OH_{(S)} \rightarrow H_2O + O_{(S)} & (1.3) \\
2CH_3O \rightarrow 2CH_2O + 2H_{(S)} & (1.4) \\
2H_{(S)} \rightarrow H_2 & (1.5) \\
\hline
2CH_3OH + 1/2O_2 \rightarrow 2CH_2O + H_2 + H_2O & (1.6)
\end{array}$$

Supported silver catalysts could be used to reduce the cost, but they result in unacceptable selectivity losses. Furthermore, alloying silver with gold could improve the selectivity,[10] but commercialization of this superior catalyst is inhibited by the increased expense of such a modification.

Supported metal catalysts offer an obvious advantage over bulk metal catalysts by more effectively utilizing an expensive metal. This can be achieved by evenly dispersing fine metal particles on a high-surface-area substrate. In this catalytic system, metal particles are active agents, and the support provides a medium to deposit and immobilize these active agents. In addition, the existence of a support sometimes can substantially modify the catalytic properties of the metal. Some changes which might be triggered from metal-support interactions include:

1) Electronic properties. Small metal particles have the tendency to lose electrons to the support and thus assume a small positive charge.

2) Particle sizes and shapes being subjected to the pore sizes of support, e.g. zeolite.

3) Oxidation state. The ease of metal cation substituting into the support lattice can make a metal cation difficult to reduce to the zero-valent state.

4) Morphology. A particular metal will wet some support surfaces but not others.

5) Strong metal-support interaction (SMSI). When a noble metal is supported on a reduced metal oxide, its H_2 and CO chemisorption capacity falls dramatically.[11]

6) Co-operative mechanisms of catalysis. When the support also takes part in catalytic reaction directly, catalysis might be occurring at active sites on both the metal and the support surface, or the metal-support interface.

Despite the several possible metal-support interactions, there are situations where catalytic reactions over supported metal catalysts are not different from those on single-crystal metal surfaces. In this case, well-defined single-crystal surfaces can be utilized to study the catalysis mechanism.

1.2.2 Oxide Catalysts

Oxide catalysts have found wide ranges of uses in, for example, dehydration of alcohols, cracking of hydrocarbons(Al_2O_3), dehydrogenation of alkane(Cr_2O), reforming(Mo/Al/O), methanol synthesis(Cu/Zn/O), sulfuric acid synthesis(K/V/O), and selective oxidation(Fe/Mo/O, V/P/O). Usually these oxide catalysts don't need supports, but there are some exceptions. A few important factors were found that can affect the activity of oxide catalysts.

1) Density (e.g. diluted, concentrated) of transition metal ions. [12]

2) Site (e.g. octahedral, tetrahedral) of transition metal ions.[13]

3) Surface properties (e.g. density of active sites, dangling bonds, special defects), [14] which are always of paramount importance for all heterogeneous catalysts.

4) Bulk properties (e.g. electronic mobility, oxygen diffusion), which are of particular importance for selective oxidation and ammoxidation catalysts.[15] In both cases, the oxide catalysts work as a regenerable reagent and as a reservoir for electrons and oxygen, which therefore should readily flow from one site to another.

A molybdate catalyst is also utilized for conversion of methanol to formaldehyde commercially. The major difference from using a silver catalyst is that the hydrogen from the methoxy group is abstracted by silver metal in the one case and by a surface oxygen in the case of the molybdate catalyst. Molybdates and vanadates are among the most widely used selective oxidation catalysts. The former are frequently supported on alumina, and the latter are sometimes supported on titania. Silica sometimes is used as a binder to provide strength rather than as a support to provide dispersion.

1.2.3 Zeolites

Zeolites, crystalline aluminosilicate with general formula $M_{x/n}[(AlO_2)_x(SiO_2)_y].mH_2O$, are probably the most well-known and most widely used catalysts in industry. Unlike the above mentioned catalysts, zeolites represent a unique class of well-defined microporous materials used as heterogeneous catalysts with vast cavities accessible to reactants. Thus distinguishing between bulk and surface properties becomes much less meaningful.

Zeolites are considered as a special type of catalyst possessing shape selectivity due to their regular pores of molecular dimensions, exceptional acidity when Al^{3+} is present instead of Si^{4+}, and great capability for ion exchange. This shape selectivity can be exhibited in three different ways:

1) Reactant-selective catalysis: catalyzing only the reaction of certain small molecules in a reactant mixture;

2) Product-selective catalysis: allowing only the smaller products of a reaction to leave, while larger molecules can stay behind and continue to react;

3) Transition-state-selective catalysis: blocking a particular reaction by inhibiting a very large intermediate produced in the cavity.

The number of acid sites within a zeolite pore is proportional to the aluminum content in the framework, providing all interstitial cations have been eliminated.[16] These could be either Brønsted acid sites (when both proton and aluminium have same concentration, i.e.$H_xSi_{1-x}Al_xO_2$) or Lewis acid sites (when proton concentration drops below the aluminium concentration, as occurs during severe dehydration)(Figure 2). Both Brønsted acid sites and Lewis acid sites may be utilized for catalysis such as, for example, cracking of petroleum. Further discussion of zeolites comes in section 1.3

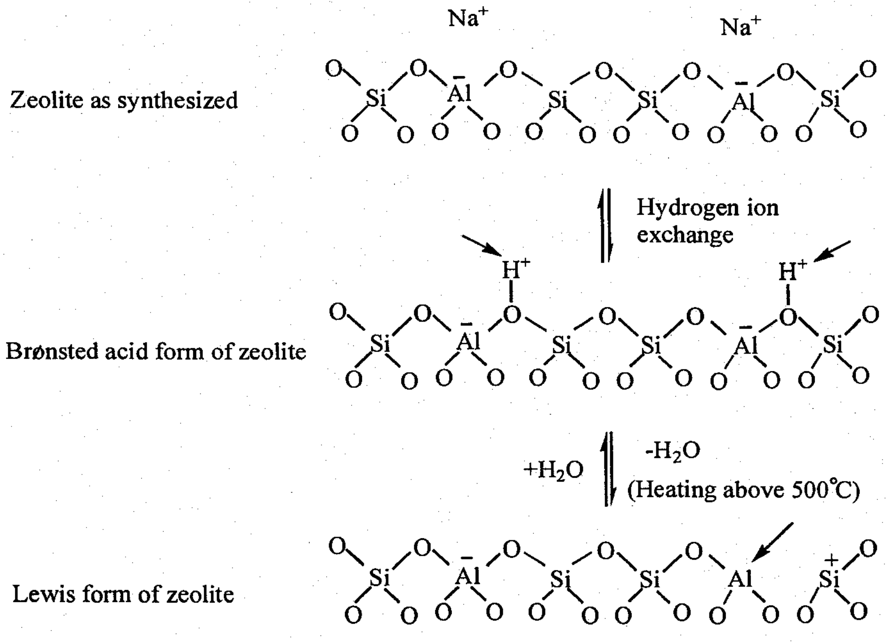
Na⁺
Na⁺
Zeolite as synthesized
Hydrogen ion exchange
H⁺
H⁺
Brønsted acid form of zeolite
+H₂O
-H₂O
(Heating above 500℃)
Lewis form of zeolite
Si
Al
O

Figure 2. Scheme for the generation of Brønsted and Lewis acid sites in zeolites. (Adapted from Smart, L. and Moore, E. *Solid State Chemistry-An Introduction*, 2nd edition, **1992**)

The ion exchange of interstitial cations with several different cations can be used to adjust the acidity, shape selectivity properties of zeolites, to increase stability, and also to add additional catalytic functions into zeolites.

Zeolites can be naturally occurring, for example faujasite, or synthesized under hydrothermal conditions, such as ZSM5. The synthetic ZSM5 zeolite, discovered by Mobil [17] with channels diameters of about 5Å, is currently being used in a process to convert methanol directly to gasoline, and for xylene isomerization.

1.2.4 Sulfide catalysts

Sulfide catalysts are widely used for hydrodesulphurization to remove sulfur from natural gas, petroleum, and coal, etc. before chemical processing or fuel utilization, and therefore are of great importance. This reaction can be schematically represented as

$$\text{-CH-S-} + 2H_2 \rightarrow \text{-CH}_3 + H_2S \qquad (1.7)$$

Cobalt molybdate supported on Al_2O_3 (cubic phase) represents such a commonly used sulfide catalyst.[18]

1.3 Development History of Mesoporous Materials

The engineering and synthesis of porous materials with precisely controlled pore dimensions is currently a challenge in solid-state chemistry. Given the properties of narrow pore size distribution and readily tunable pore size over a wide range, these materials are ideal for catalysts, adsorbents and molecular sieves, etc.

According to International Union of Pure and Applied Chemistry (IUPAC), all the porous materials can be classified into three groups based on their predominant pore size (d):

- Microporous, d < 2nm
- Mesoporous, 2nm < d < 50nm
- Macroporous, d > 50nm

At present, macroporous materials are of relatively limited application due to their low surface area and non-uniform pores. Microporous zeolites, featured with their large surface area, high thermal/hydrothermal stabilities, tailored concentration and strength of active sites, and variable intricate channel structure, are suitable for size-specific applications in catalysis and separation.

However, zeolites show obvious limitation in processing of large size reactants. This is because they use metal ions, organic ions, or molecules as their structure templates while crystallizing, which can be reflected by their extremely narrow pore size distributions in the range of 3 to 13 Å.[19] This consequently intrigued the scientists to develop new materials which maintain the specific advantages of zeolites, while extending their pore dimension into the mesopore regime.

The breakthrough was finally made in 1992 by researchers in Mobil Oil Research and Development after they demonstrated a new approach to the synthesis of a series of large pore silicate termed M41S.[20, 21] Instead of ion or molecule templates, as in the case of zeolites, these new materials use regularly arranged crystalline micelles of surfactant molecules, which are formed by self-assembly, to direct their structure. Inorganic silicate or aluminosiicate species occupies the continuous solvent (water) region to create inorganic walls enclosing the template molecules. A so-called "liquid crystal templating" mechanism was proposed to be operative during the synthesis of these mesoporous materials. This mechanism is strongly supported by two experimental discoveries:

1) The pore sizes of M41S materials are directly dependent on the alkyl chain length of surfactant;

2) In addition to hexagonal MCM-41, cubic (MCM-48) and layered (MCM-50) crystallization products, directly corresponding to cubic and lamellar liquid crystal phases, were also synthesized.[22]

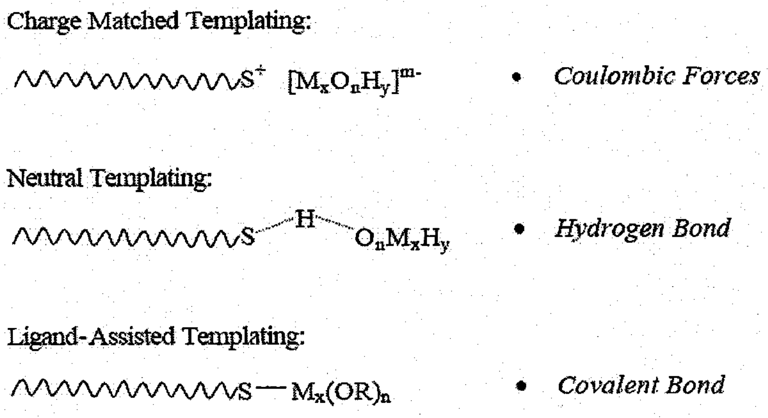
Charge Matched Templating:
S^+ $[M_xO_nH_y]^{m-}$
• Coulombic Forces
Neutral Templating:
$S \cdots H \cdots O_nM_xH_y$
• Hydrogen Bond
Ligand-Assisted Templating:
$S—M_x(OR)_n$
• Covalent Bond

Figure 3. A schematic overview of three liquid crystal templating models. (Adapted from ref. 31)

While it's possible that, in the formation of MCM-41, the surfactant phase acts as template for inorganic assembly either by preformed micelles, or the introduction of inorganic silicate species itself mediates the hexagonal ordering, Stucky and co-workers generalized the latter mechanism to a dynamic, charge matching templating approach based on the compensation of ionic charges,[23-26] which demonstrate that the inorganic species can promote the formation of the liquid crystal phase below the critical micelle concentration (CMC). A neutral templating approach was also proposed by Pinnavaia and co-workers based on hydrogen-bonding interactions and self-assembly between neutral primary amine micelles and neutral inorganic precursors.[27-29] Later on, Antonelli and

Ying developed a ligand-assisted templating route to mesoporous transition metal oxides using covalent bonding.[30-34] (Figure 3) In addition, by using amphiphilic poly (alkylene oxide) block copolymers as structure-directing agents, a very large-pore (up to 140Å) mesoporous material was reported by Stucky and co-workers.[35, 36]

While siliceous mesoporous materials attract much attention following the discovery of M41S materials, there was special interest in developing mesoporous transition metal oxides because transition metal oxides possess a much wider range of physical properties in applications such as optics, electronics and sensing, etc. Stucky and co-workers[23, 24, 37] first reported mesostructured tungsten oxides in 1994 by using the charge matching approach, but unfortunately, most of these phases were lamellar and the few mesostructures were thermally unstable, collapsing upon surfactant removal.

The big breakthrough in this area came in 1996 when Antonelli and Ying developed the ligand-assisted templating approach.[30-33] This novel approach used a dative coordinate bond interaction between long-chain amine surfactant molecules and metal alkoxides, followed by selective hydrolysis and condensation of the mixture (Figure 4). No preformed micelles were required as in the case of M41S. However, it is important that the surfactant-precursor bond is strong enough to resist hydrolysis, but at the same time allowing easy chemical removal of the template after synthesis without damage to the mesostructure. Based on this approach, a new family of mesoporous transition metal oxide molecular sieves, termed M-TMS1 (M=Nb, Ta, Ti, Zr), were synthesized possessing high surface area and remarkable thermal stabilities, and are now being explored for their versatile applications in industry.

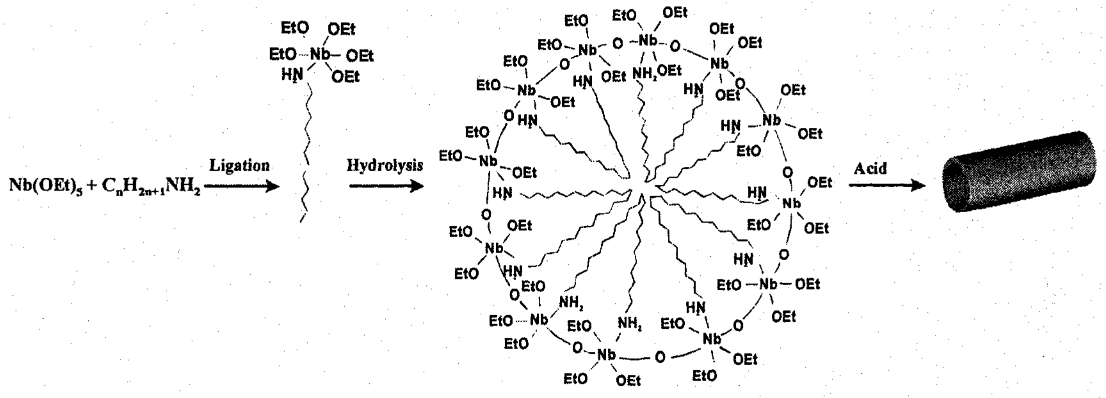

Figure 4. Schematic representation of possible synthesis pathway for Nb-TMS1 under a ligand-assisted templating mechanism. (Adapted from ref. 32)

1.4 Current Status of Mesoporous Transition Metal Oxides as Catalysts

One of the most obvious fields for use of these mesoporous materials is catalysis. A lot of catalytic experiments have been performed on mesoporous silica/aluminum silicate based catalysts since the discovery of M41S.[38] In most of the cases, the mesoporous materials function as a substrate incorporated with other active agents (e.g. metals, or metal oxides). However, in general, these ordered mesoporous materials are of comparably less interest because the advantage of sharp pore size distribution and regular pore arrangement doesn't help to improve the activities remarkably; furthermore, cheaper, easily synthesized, and almost as good alternatives are always available. On the contrary, there are often no good alternative routes for the synthesis of high surface area transition metal oxides, and the added cost incurred by mesostructuring is relatively less important, when compared with the advantages they bring such as, for example, finely tuned pore size, metal oxide wall structures and compositions, high surface areas and enhanced accessibility of the active surface sites. In addition, the variable oxidation states of transition metals are another crucial advantage over siliceous M41S for redox catalysts. However, despite these facts which suggest promising catalytic applications of ordered mesoporous transition metal oxides, so far only a few reports are available on their catalytic performance. These are summarized in Table 2.

Table 2. Up to date studies of mesoporous metal oxides in catalysis.

Mesoporous system	Conversional system	Reaction	Activity/ selectivity	Reasons responsible for the change
MesoporousTiO_2 film [39]	Gel film	Photooxidation of NO to NO_2	↑	Higher surface area
NiO doped mesoporous Ta_2O_5 [40]	Amorphous/ crystalline NiO-Ta_2O_5	Photocatalytic water decomposition to $H_2 + O_2$	↑	Higher surface area & better NiO dispersion
Phosphated mesoporous TiO_2 & Nb_2O_5 [41]	Bulk anatase phase	Photocatalytic 2-propanol dehydrogenation to acetone	↓	Amorphous walls & surface defects
Fe_2O_3 incorporated mesoporous TiO_2 [42]	Non-porous Fe_2O_3- TiO_2	Cyclohexane oxidation to cyclohexanol & cyclohexanone	5% ↑	Higher surface area & improved dispersion of surface active sites
VOx incorporated mesoporous TiO_2 [43]	Non-porous TiO_2 matrix	Propene oxidation to $CO + CO_2$	18 times ↑	
Mesostructured VPO [44]	Organic, well-crystallized VPO	n-butane oxidation to maleic anhydride	Selectivity 10% ↓	Limited thermal stability

1.5 Nitrogen Activation

Molecular nitrogen N_2 is abundant in nature yet very inert due to the strength of its triple bond (940kJ/mol), nonpolarity and high ionization potential (15.058eV). The process that takes dinitrogen from the atmosphere into the biosphere in a usable form, i.e.

high-value nitrogen-containing products, is referred to as nitrogen fixation or activation. Nitrogen activation is such an important process because nitrogen atoms are not only essential for the function of biological molecules, but they are an important component of fertilizers and medicaments as well. Additional uses are related to dyes, explosives, and resins. Generally, nitrogen activation falls into three parallel fields: biological, homogeneous, and heterogeneous.

Interest in biological nitrogen fixation was stimulated by the observation that some soil-dwelling bacteria could fix nitrogen at room temperature. The activation process is known to be accomplished by a class of enzymes called nitrogenases [45] which consist of two units - an iron-containing protein and a Fe-Mo protein. Once N_2 binds to enzyme complex, it is reduced by a series of six electron transfers. The electrons originate from the degradation of photosynthetic carbohydrate and are carried to the nitrogenase enzyme complex by a reduced ferredoxin. Protons for the formation of ammonia are generated

$$N_2 + 6H^+ + 6e^- \rightarrow 2NH_3 \qquad (1.8)$$

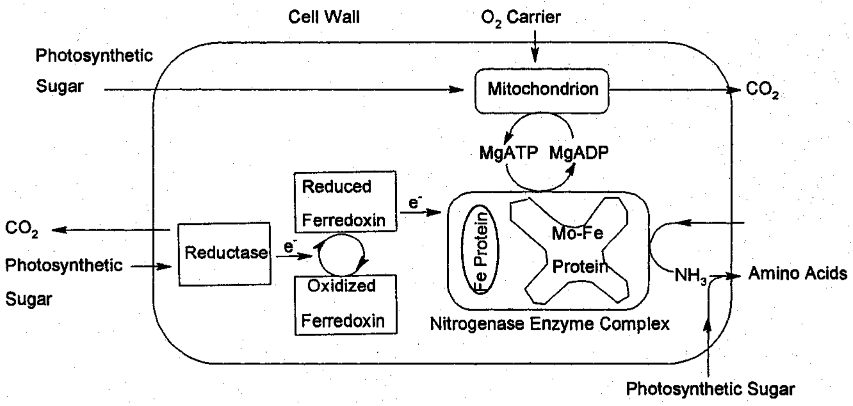
Cell Wall
O_2 Carrier
Photosynthetic Sugar
Mitochondrion
CO_2
MgATP
MgADP
Reduced Ferredoxin
e^-
CO_2
Photosynthetic Sugar
Reductase
e^-
Oxidized Ferredoxin
Fe Protein
Mo-Fe Protein
NH_3
Amino Acids
Nitrogenase Enzyme Complex
Photosynthetic Sugar

Figure 5. Schematic representation of a typical bacterial nitrogen-fixing system. (Adapted from Butler, I. S. and Harrod, J. F. *Inorganic Chemistry: Principles and Applications*, The Benjamin/Cummings Publishing Company, **1989**)

through hydrolysis of MgATP to give MgADP and H_3PO4. MgATP is regenerated at a mitrochodrion where the oxidation of carbohydrate by oxygen is carried out (Figure 5).

Although the crystal structure of the Fe-Mo active site of certain nitrogenase enzymes has been characterized,[46-48] little progress has been made so far to determine the mechanism of how N_2 is taken and then converted to NH_3 step by step. Nevertheless, interest remains in modeling this process through biomimetic approaches.

1.5.1 Homogeneous Nitrogen Activation

Research in nitrogen activation under homogeneous conditions plays a very important role in exploring the mechanism. This is usually performed by using well-defined organometallic compounds as catalysts. The classic work from this field has shown that this process depends on the metal center, the ligands, as well as the acid used and the solvent.[49] Coordination of molecular nitrogen to transition metal complexes can truly activate strong N-N bond at mild conditions. Characterization (e.g. X-ray crystallography, NMR) of each intermediate therefore may give us a very good picture about how this activation is achieved, most importantly, how ammonia could be produced upon stoichiometric protonation and even catalysis.

In 1995, Cummins and co-workers reported the most impressive example of direct cleavage of N≡N triple bond to two nitride(N^{3-}) ligands in its reaction with $Mo(NRAr)_3$, where R is $C(CD_3)_2CH_3$ and Ar is 3,5-$C_6H_3(CH_3)_2$ (Figure 6).[50] The reductive scission of the N≡N triple bond relies on formation of N≡Mo triple bond, one of the strongest metal-ligand bonds [51] which clearly provides the thermodynamic driving force, as well as a soluble dimolybdenum intermediate with a bridging dinitrogen ligand (compound 3). Although this purple intermediate was not isolated and analyzed by X-ray crystallography, it was observed spectroscopically.

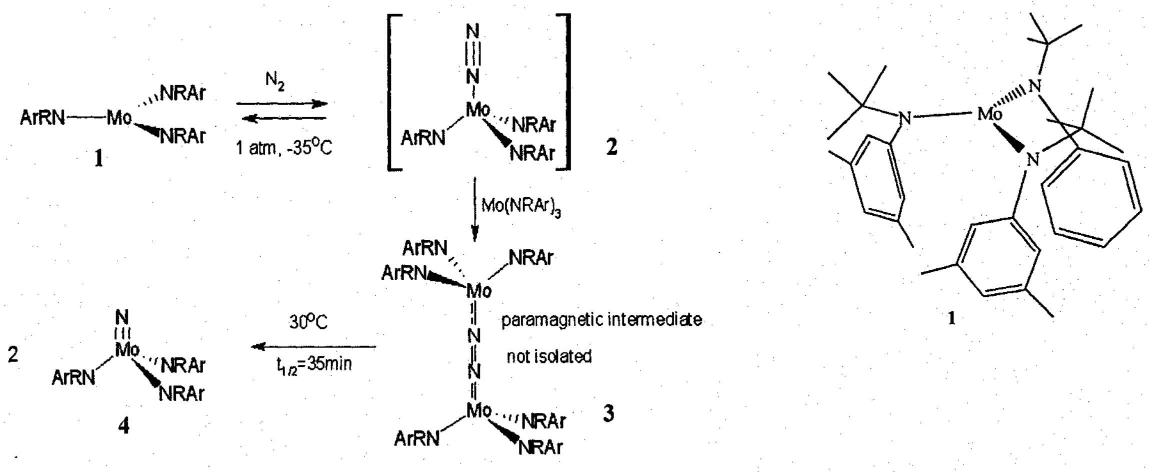
ArRN—Mo NRAr NRAr
1
N2
1 atm, -35°C
N≡N Mo ArRN NRAr NRAr
2
Mo(NRAr)3
ArRN ArRN NRAr Mo
paramagnetic intermediate
not isolated
N=N Mo ArRN NRAr NRAr
3
30°C
t1/2=35min
2
N≡ Mo ArRN NRAr NRAr
4
N Mo N N
1

Figure 6. Proposed reactions for dinitrogen cleavage over a three–coordinate molybdenum (III) complex. (Adapted from ref. 50)

Instead of simple displacement of coordinated N_2 by H_2, which is the most common case, Fryzuk and co-workers demonstrated, in 1997, that a side-on bound dinitrogen zirconium complex $\{[P_2N_2]Zr\}_2(\mu\text{-}\eta^2\text{-}N_2)$ could heterolytically cleave dihydrogen to form an N-H unit and a bridging hydride(Figure 7, compound 2).[52] In this case, the dinitrogen fragment was assumed to be strongly activated as N_2^{4-} and bound to two Zr^{4+} centers. A similar transformation of coordinated dinitrogen by reaction with primary silances was also observed due to the close analogy between H-H and Si-H bonds, which resulted in the formation of silylhydrazido species with a bridging hydride $([P_2N_2]Zr)_2(\mu\text{-}\eta^2\text{: }\eta^2\text{-}NNSiH_2Bu^n)(\mu\text{-}H)$. This obtained butylsilyl analogue was isolated from toluene as yellow needles and its solution characteristics are very similar to those solution structure for compound 2, therefore supporting the proposed solution structure of $([P_2N_2]Zr)_2(\mu\text{-}\eta^2\text{: }\eta^2\text{-}NNH)(\mu\text{-}H)$ (compound 2).

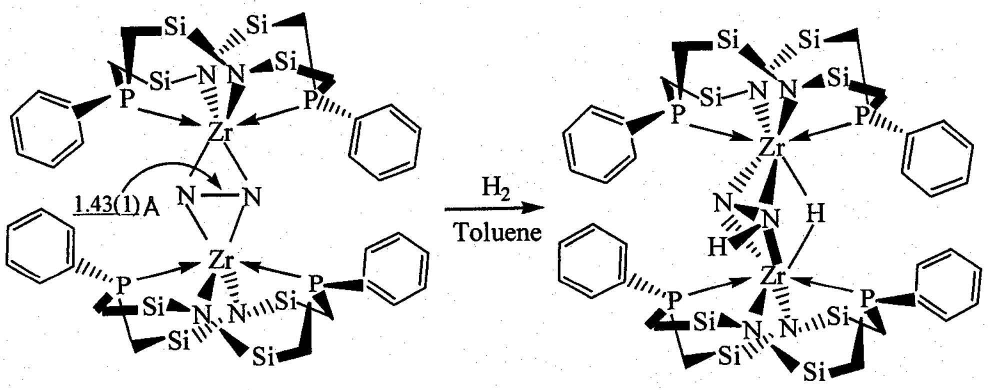

1   **2**

Figure 7. Reaction of dinulear zirconium complex with H_2 to form a N-H unit and a bridging hydride. (methyls on the Si atoms have been omitted for clarity)

(Adapted from ref. 52)

In spite of all this progress in dinitrogen bond cleavage, hydrogenation, and nitrogen derivatives (e.g. diazenido, hydrazido) functionalization, the discovery of a catalytic system remains challenging. Why? Because the synthesis of dinitrogen complexes usually needs strongly reducing conditions, and the typical reaction patterns of a coordinated dinitrogen moiety involve electrophiles, which could short-circuit the desired process and make realization of a catalytic cycle problematic.[53]

A major advance toward unraveling the stepwise catalytic reduction of dinitrogen to ammonia was achieved in 2003. Schrock and co-workers proposed probably the most mechanistically elaborated system at a single molybdenum center.[54] By introducing novel tetradentate $[HIPTN_3N]^{3-}$ triamidoamine ligand (hexa-iso-propyl-terphenyl, 3,5-(2,4,6-i-$Pr_3C_6H_2)_2C_6H_3$) to the catalyst, and carefully employing {2,6-lutidinium}{BrAr'$_4$} as the proton source and decamethyl chromocene as the reductant, they could achieve high efficiency of 66% NH_3 yield. Extensive ^{15}N labeling studies, nuclear magnetic resonance (NMR) studies and X-ray crystallography were used to fully characterize six

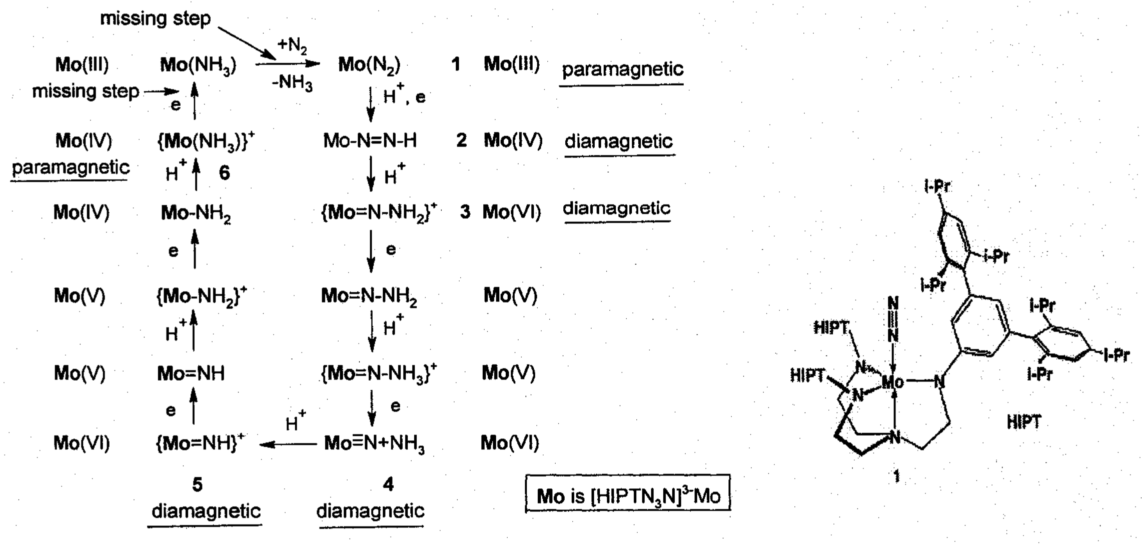
missing step
+N2
Mo(III)
Mo(NH3)
-NH3
Mo(N2)
1 Mo(III) paramagnetic
missing step
e
H+, e
Mo(IV)
paramagnetic
{Mo(NH3)}+
H+ 6
Mo-N=N-H
2 Mo(IV) diamagnetic
H+
Mo(IV)
Mo-NH2
{Mo=N-NH2}+
3 Mo(VI) diamagnetic
e
e
Mo(V)
{Mo-NH2}+
Mo=N-NH2
Mo(V)
H+
H+
Mo(V)
Mo=NH
{Mo=N-NH3}+
Mo(V)
e
H+
e
Mo(VI)
{Mo=NH}+
Mo≡N+NH3
Mo(VI)
5
diamagnetic
4
diamagnetic
Mo is [HIPTN3N]3-Mo
i-Pr
i-Pr
i-Pr
i-Pr
i-Pr
i-Pr
N
N
HIPT
HIPT
HIPT
Mo
N
N
N
N
1

Figure 8. Proposed intermediates in the reduction of dinitrogen at a single molybdenum center through the stepwise addition of protons and electrons. (Adapted from ref. 54)

intermediates participating in the catalytic reduction of end-on bound N_2 step by step, alternating addition of six protons and six electrons (Figure 8). However, this potentially catalytic process was not complete because two steps in this cycle are missing which include 1) reduction of {**Mo**(NH_3)}{BrAr'$_4$} to **Mo**(NH_3); and 2) displacement of ammonia from **Mo**(NH_3) by dinitrogen.

In 2004, Chirlk and co-workers reported their extensive work on zirconium complexes containing cyclopentadienyl ligands and showed that the first direct observation of N-H bond formation from N_2 and H_2, coupled with either N_2 cleavage of intermediate $[(\eta^5\text{-}C_5Me_4H)_2ZrH]_2(\mu_2, \eta^2,\eta^2\ \text{–}N_2H_2)$ at 45°C, or full hydrogenation to ammonia with 10-15% yield at 85°C (Figure 9).[55]

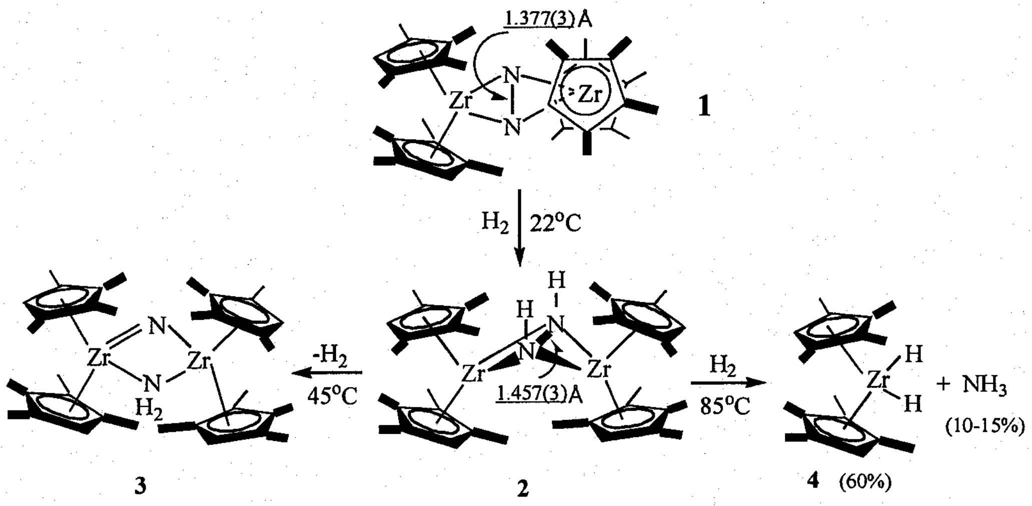

Figure 9. Scheme for hydrogenation of dinuclear zirconium complex and cleavage of N_2. (Adapted from ref. 55)

As we know that most dinitrogen complexes display end-on mode coordination in both terminal and bridging modes, side-on bound dinitrogen complexes also commonly exist as dinuclear metal systems with only one exception.[56] In 2001, Fryzuk and co-workers reported a very interesting tantalum complex that combines both the side-on and end-on modes. Dinuclear tantalum tetrahydride complex $([NPN]Ta)_2(\mu\text{-}H)_4$(where NPN=$PhP(SiMe_2CH_2NPh)_2$) reacts with dinitrogen at room temperature and pressure to generate the bridging, side-on end-on dinitrogen complex $([NPN]Ta)_2(\mu\text{-}H)_2(\mu\text{-}\eta^2,\eta^1 - N_2)$(Figure 10).[57] This reaction is remarkable since a dinitrogen complex is synthesized under mild conditions and avoids using a strong reducing agent. Furthermore, unlike many other dinitrogn complex formed by the reductive elimination of H_2, the dinitrogen moiety in this complex is strongly activated (N-N bond distance 1.319 Å), since the Ta-Ta bond in $([NPN]Ta)_2(\mu\text{-}H)_4$ offers two more electrons for the reduction of the dinitrogen moiety.

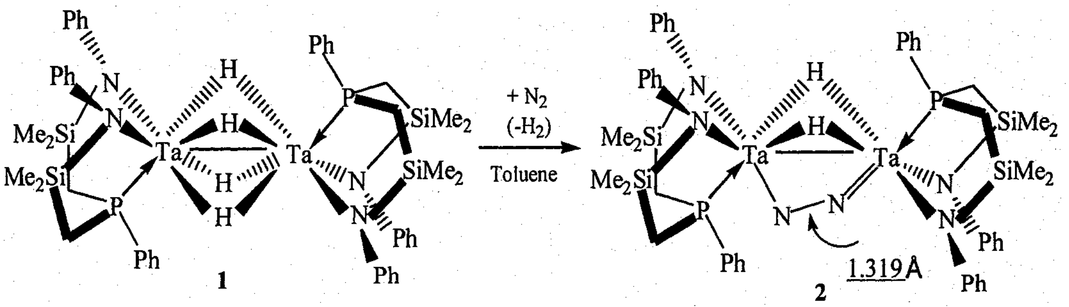

Figure 10. Scheme for formation of both side-on and end-on dinitrogen coordination from a dinuclear tantalum complex. (Adapted from ref. 57)

1.5.2 Heterogeneous Nitrogen Activation - Haber-Bosch Process

Heterogeneous catalysis plays a key role in chemical industry as mentioned in section 1.1. However, unlike well-defined homogeneous catalysts, most heterogeneous catalysts of industrial importance are multicomponent materials that are designed by trial-and-error experimentation. Application of even the most sophisticated physical-chemical characterization techniques is usually not sufficient to fully elucidate the reaction mechanism.

Haber-Bosch process is responsible for the industrial source of ammonia. It operates under reaction temperature of around 400°C and total pressure of 150-300 atm. over a Fe-based catalyst system.

$$N_2 + H_2 \rightarrow 2NH_3,\ \Delta H^0_{298} = -46.1\text{kJ/mol} \qquad (1.9)$$

The triply promoted Fe-based catalyst system mainly consists of Fe_3O_4 (94 wt%), Al_2O_3(2.3 wt%), K_2O(0.8 wt%), and CaO(1.7 wt%). Among them, alumina acts as structural promoter, preventing iron crystallites from sintering; K_2O functions as chemical promoter, enhancing the specific reaction rate by donating electrons; CaO is just used to remove silica impurities which would otherwise combine with an alumina promoter and poison the catalyst.

1.5.2.1 Mechanism and Kinetics

The overall reaction can be written as following elementary steps (* represents an active center): [58]

$$N_2(g) + * \leftrightarrow N_2\text{-}* \qquad (1.10)$$

$$N_2\text{-}* + * \leftrightarrow 2N\text{-}* \qquad (1.11)$$

$$H_2(g) + 2* \leftrightarrow 2H\text{-}* \qquad (1.12)$$

$$N\text{-}* + H\text{-}* \leftrightarrow NH\text{-}* + * \qquad (1.13)$$

$$NH\text{-}* + H\text{-}* \leftrightarrow NH_2\text{-}* + * \qquad (1.14)$$

$$NH_2\text{-}* + H\text{-}* \leftrightarrow NH_3\text{-}* \qquad (1.15)$$

$$NH_3\text{-}* \leftrightarrow NH_3(g) + * \qquad (1.16)$$

The elementary reaction starts with nitrogen molecule adsorbs at an active center on an iron surface, for example Fe(111), then the dissociation of adsorbed nitrogen proceeds gradually while simultaneously forming Fe-N chemisorption bonds. Hydrogen, at the same time, could also be easily atomized by iron. The chemisorbed N atom thus readily reacts with atomized hydrogen to produce NH, NH_2, and finally NH_3, which then desorbs from the surface into the gas phase, and leaves active centers available for the next reaction cycle.

Kinetic studies showed that among these elementary reactions, the dissociative adsorption of nitrogen on the catalyst surface, i.e. step 1.11, is the rate-limiting reaction because the total rate of the reaction equals the dissociation rate of N_2 at low conversions. The low rate of ammonia synthesis is mainly attributed to the very low N_2 dissociative sticking probability, in the range of 10^{-7}~10^{-6}, which also explains why high pressure benefits the reaction 1.10. The proposed net activation energy for the reaction is about 76kJ/mol.

Iron is an effective catalyst for ammonia synthesis, because it lowers the barrier to N_2 dissociation. More importantly, the thus formed Fe-N bond has just the right bond strength. If the metal-nitrogen (M-N) is too strong, as in the case of early transition metals, an inert surface nitride could form, which will hinder further reactions proceeding. On the contrary, if the M-N bond is two weak, the chemisorbed atomic nitrogen N(a) might have very short surface residence time, which will result in combination of two N(a) and formation of N_2 instead of NH_3, this certainly lowers the efficiency of the catalyst.

1.5.2.2 Structure Sensitivity of Fe Catalyst

It is generally accepted that the Fe catalyst in ammonia synthesis is structure-sensitive. This means, classically, that the reaction rate is dependent on the particle size of catalyst. More precisely, it indicates that the reaction rate varies according to different surface orientation. Experimental results using a single-crystal iron sample under ultra-high vacuum (UHV) conditions showed the reactivity of five crystal faces in the sequence Fe(111) > Fe(211) > Fe(100) > Fe(210) > Fe(110)(Figure 11, Table 3). It was suggested that the active sites C_7 (Fe atoms with seven nearest neighbors) are crucial factors responsible for the reactivity difference.[59]

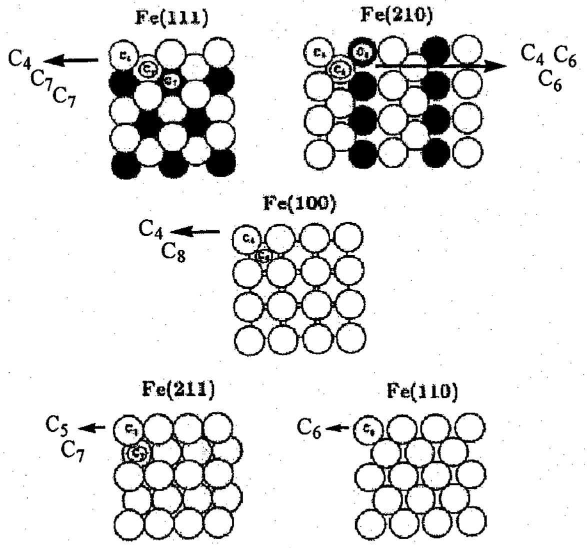

Figure 11. Schematic representations of the idealized surface structure of the (111), (211), (100), (210), and (110) orientation of iron single crystals. The coordination of each surface atom is indicated. (Adapted from ref. 60)

Table 3. Reactivity of five Fe crystal faces.

Face	Fe(111)		Fe(211)		Fe(100)		Fe(210)		Fe(110)
Activity		>		>		>		>	
Layer(s) exposed	3		2		2		3		1
C_7 sites	Yes		Yes		No		No		No

1.5.2.3 Effects of Aluminum Oxide

Aluminum oxide is known as a structure promoter in the catalytic system. However, simply depositing aluminum oxide on an iron catalyst only results in a decrease of the rate of ammonia synthesis in direct proportion to the amount of surface covered. This suggests that in order to exert the structure promoter effect, aluminum oxide must participate in the reaction with iron. In commercial production of ammonia, this is done by fusion of 2-3% by weight of aluminum oxide with iron oxide (Fe_3O_4).

1.5.2.4 Effects of Potassium

Effects of Potassium, the chemical promoter, can be summarized as: [60]

1) Promoting the sticking coefficient of nitrogen chemisorption and assisting in making all exposed surfaces of the iron particles equally reactive, e.g. a factor of 280× enhancement on Fe(100) versus 10× enhancement on Fe(111).

2) Increasing the adsorption energy of molecular nitrogen. Strong ionic characteristics of the potassium-iron bond increase the local ionization potential of the surface iron atom. Therefore, more electron density transfers to the nitrogen $2\pi^*$ antibonding orbitals from the surface, thus lower activation barrier for nitrogen dissociation. Because of their great electron donating property, these alkali metal or alkaline earth metal promoters are called electronic promoters.

3) Lowing the adsorption energy of ammonia products. The TPD of ammonia was performed on clean Fe(111) and K/Fe(111), which shows that the desorption maximum shift to lower temperature when potassium is coadsorbed on the surface. Therefore, the residence time for the adsorbed ammonia is reduced and more of the active sites are available for the dissociation of nitrogen.

1.5.3 Ru-based Catalyst-the Second Generation

Haber-Bosch process is one of the most important discoveries in 20th century considering that ammonia accounts for the second largest inorganic chemical production after sulfuric acid. However, the production of ammonia is also quite an energy-consuming process, which is responsible for more than 1% of global energy consumption; [61] therefore, finding a more efficient and energy-saving alternative process has long been one of the biggest challenges in modern catalysis, which has profound implication not only for fossil-fuel consumption but the worldwide economy as well.

A second generation of Ru-base catalysts is the best candidates so far for Haber synthesis. In fact, a new ruthenium-active carbon-alkali metal system became commercially applied in the Kellogg Advanced Ammonia Process (KAAP) in 1990s. [62] This catalyst system allows ammonia produced at low temperature and pressure and thus reduces the energy costs.

When compared with the iron catalyst, the ruthenium-based catalysts possess the following characteristics:

1) The Ru/AC-K catalyst shows 10-fold increase in activity over the conventional Fe catalyst at the same operating condition. [63]

2) The dissociative chemisorption of nitrogen is still the rate-determining step in the case of the Ru catalysts. But contrary to the Fe catalyst, there is no indication of molecularly

chemiadsorbed nitrogen,[64] so that elementary reactions 1.2 and 1.3 combine together and become one reaction:

$$N_2(g) + 2^* \leftrightarrow 2N\text{-}^* \qquad (1.17)$$

3) Kinetic studies show that the ruthenium catalyst has a lower sticking coefficient for nitrogen than the iron catalyst, which is on the order of 10^{-12}, and independent of ruthenium surface orientation. [64] This means that the ruthenium catalyst is not quite as structure sensitive as the Fe catalyst.

4) The order in hydrogen becomes negative [65, 66] as compared to a positive order in the case of the iron catalyst, which demonstrates an inhibiting effect of hydrogen on ammonia synthesis. Under synthesis conditions, greater coverage of H* rapidly saturates the ruthenium surfaces and thus blocks the N_2 adsorption sites (active surface sites), although higher coverage by atomic hydrogen can accelerates stepwise hydrogenation of N*.

5) Because ruthenium is a more expensive metal, a high surface area support is preferred on which ruthenium metal can be finely distributed as very small crystals. Only in this case, can large fractions of the metal atoms be exposed to the reactant gases and productive catalytic activity be realized for low concentrations (e.g. 1-2%) of this expensive metal catalyst.

There is no doubt that ruthenium is a superior catalyst to iron for ammonia synthesis. For this reason, the exploration of different catalyst supports and promoters which can best match ruthenium have been ongoing in an effort to further improve the catalyst.

The pioneering work on activity of Ru-K/AC was done by Ozaki in 1970s.[63] Active carbon (A.C), with high surface area of $1068 m^2/g$, can hold potassium by formation graphite-potassium complex. In addition, active carbon acts as a medium to transfer electrons from alkali to ruthenium because of its electron withdrawing property.

This Ru-K/AC catalyst system was quite successful, and then developed for commercial use in 1990s. However, there are two major drawbacks in this system: 1) Potassium metal is highly sensitive to water and oxygen, which makes it difficult to handle in a large scale, therefore, $RbNO_3$ was considered as a replacement although less effective; [67] and 2) ruthenium also catalyzes the oxidation and methanation of carbon,[68, 69] for this consideration, zeolites and a series of oxides have been explored.

Zeolites are of particular interest as support candidates of the Ru catalyst system, they provide a few special advantages such as 1) the location of ruthenium particles and alkali metal cations are relatively well defined, 2) sizes of ruthenium particles are limited to the sizes of zeolite micropores or cages, therefore, the fraction of ruthenium exposed was greater than those of nonzeolitic catalysts, 3) the nature of the cation can be readily modified, and 4) the interaction between Ru particles and the strong ionic potential of the zeolite surface offers additional electronic modifications, which are not available in other catalytic systems.

By examining ruthenium zeolite X and zeolite Y systems, Ciseneros and Lunsford found RuKX being the most active catalyst in the sequence of RuKX>RuNaX>RuCsX, and a RuKX zeolite was much more active than the RuKY one.[70] They reached the conclusion that activity of faujasite zeolite-supported ruthenium catalysts strongly depends on the zeolite type (Si/Al ratio), the kind of cation present in the zeolite, as well as the size of the Ru particles.

Al_2O_3 and MgO supported Ru catalysts were mainly studied by Aika and co-workers, and Ru-Cs/MgO is by far one of the most promising catalytic systems for ammonia synthesis.[71, 72, 73] The authors concluded that the high activity of Ru-Cs/MgO catalyst comes from combination of the high dispersion of Ru particles on MgO surface, use of

Cl-free Ru precursor and basicity of MgO support. This last factor results in a favorable weak interaction between support and promoter, thus enhancing the interaction of the promoter and Ru. Surprisingly, lanthanum is the best promoter for Al_2O_3, which was explained by lanthanides being strong metal-support interaction (SMSI) oxides.[74]

Davis and co-workers also performed studies on Ru catalysts supported on zeolite X, MgO, as well as pure silica MCM-41[75] and demonstrated a RuCsX catalyst could be made with higher activity than that of a RuKX by maximizing Cs loading into the zeolite X catalyst, a result consistent with the rank of promoter basicity. In both of zeolite X and MCM-41 systems, barium becomes the best promoter. The authors also discovered that in the presence of Ba, the apparent activation energy of Ru/MgO can be decreased markedly. But this is not applicable for the RuBaX system, which suggests that this effect is not due entirely to the existence of barium, but instead presumably is caused by the combined interactions of the promoter, the support, and the ruthenium metal.

Explanation for the effects of the support and promoter on catalytic activity are a matter of contention.[75] In general, surface reactions among Ru particles, the support, and the promoter (MO) should be considered:

$$\text{Ru} + \text{MO} \leftrightarrow \text{Ru-OM} \qquad (1.18)$$

$$\text{Support} + \text{MO} \leftrightarrow \text{Suppot-OM} \qquad (1.19)$$

$$\text{Ru} + \text{Support} \leftrightarrow \text{Ru-Support} \qquad (1.20)$$

1.6 Nitrogen Activation on Bis-toluene Ti/Nb Reduced Mesostructure Systems

While nitrogen activation under mild conditions remains a challenge for modern catalysis, Antonelli and co-workers reported that mesoporous M-TMS1 (M=Nb, Ti, Ta), when carefully reduced by organometallic bis-toluene Ti/Nb, could activate atmospheric

N_2 to nitride at room temperature(Figure 12). Upon hydrolysis with ambient moisture in the wall of the mesostructure, surface ammonia can be formed and detected.[76, 77, 78] These processes use moist air as a source of protons and bis-toluene Ti/Nb as a reductant. Other work has shown that mesoporous Ta oxide with high surface area photocatalytically converts water into hydrogen and oxygen at rates higher than that of the bulk phase.[40] From these results it can be inferred that appropriately modified mesoporous Ta, Nb, and Ti oxides may function as a superior photocatalyst for dinitrogen reduction by water. This will be the second chapter of the thesis after introduction section.

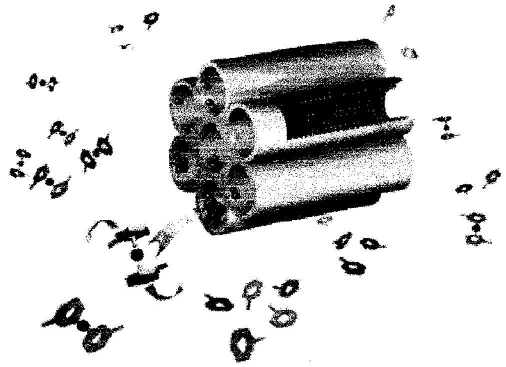

Figure 12. Schematic representation of deposition of Nb atoms from bis(toluene) niobium to the inner surface of a mesoporous oxide to form a low-valent metallic oxide coating on the internal surface. (Adapted from ref. 76)

In order to make a more efficient catalytic process, dihydrogen, which possesses a suitable reduction potential to replace bis(toluene) Ti, as well as a small size enabling better diffusion properties on surface, will be used to act as both reductant and the proton source, as in standard Haber synthesis. While mesoporous tantalum oxide has the highest thermal stability among M-TMS1 (M=Nb, Ti, Ta). In addition, pure Ta_2O_5 is of the right reduction potential to be reduced by H_2 to Ta(II)O, which then should react with N_2 according to work by our own group on reduced mesostructures as well as observations by Fryzuk [57] and Schrock.[54] However, a kinetic barrier exists for hydrogen reduction of Ta oxide. This barrier can be overcome by addition of a noble metal such as Ru or Pt. We propose that the Ru will react with the H_2 to produce electrons and protons. The electrons will reduce the Ta to a lower oxidation state, and this reduced Ta will then attack N_2 and form surface nitride just like the bis-toluene Ti/Nb reduced mesostructure systems. The nitride will then pick up protons from the H_2, which has lost its electrons to form ammonia. This process is different from standard Haber-Bosch chemistry in which all steps occur on the Ru surface. It's also possible that mesoporous Ta/Ru catalysts can act as standard Haber-Bosch catalysts at higher temperature with no involvement of the variable oxidation states of Ta. Therefore, exploring these materials and their catalytic activity in N_2 reduction will constitute the third and fourth chapters of this thesis.

Chapter 2. Mesoporous Tantalum Oxide Photocatalysts for Schrauzer-Type Conversion of Dinitrogen to Ammonia*

In the past decade, a variety of photocatalytic systems using semiconducting transition metal oxides have been developed for oxidative degeneration of organic chemicals,[79, 80] fixation of carbon dioxide,[81, 82] evolution of H_2 from water,[83, 84] and reduction of metal ions.[85] Coupling the controlled pore size and high surface areas of mesoporous materials with the photocatalytic properties of many oxides would represent an important advance in terms of reaction rates and overall efficiency because of better diffusion rates and a greater number of reactive surface sites per mol of catalyst. One of the more unusual photocatalytic processes is the conversion of dinitrogen and water over a metal-doped titanium oxide catalyst. [86-88] This process uses water as the reductant with high energy UV light as the driving force and contrasts to other methods of dinitrogen activation which are the subject of much current interest.[50, 52-54, 45, 89] Initial work by Schrauzer demonstrated that electron-hole separation on Fe-doped titania led to highly reactive sites on the surface which could trap and reduce dinitrogen. Oxidation of water by the hole provided a source of protons and electrons to complete the cycle and make the process catalytic. The doping of the metal oxide was found to be a necessary step for high activity for reasons that are still not clear, but may be related to the creation of a permanent space-charge region in the material. Further work by Hoshino demonstrated that activities of n-doped titania could be increased by incorporation of a conducting polymer on the surface, creating a p-n junction which aided in the electron-hole separation, and thus increased the efficiency.[88] The rates quoted for these reactions are on the order of mmol/h/g catalyst. Since these materials are based on oxides that normally display photocatalytic activity in the bulk phase, it appears that the development of a related mesoporous transition metal oxide-based photocatalytic process for nitrogen fixation may indeed be feasible and the rate could be improved by increasing the surface area and judicious choice of dopant. However, to date there have been numerous difficulties in exploiting the surface area of mesoporous titanium in photocatalytic processes. In 1998 Stone and Davis studied the photocatalytic activity of phosphated titania based mesoporous molecular sieves.[41] The well-known oxidative dehydrogenation of 2-propanol to acetone was used as a probe to measure the photocatalytic activity of the materials. The lower photocatalytic activity of mesoporous titania compared to the anatase phase was attributed to the amorphous nature of the walls of these materials and the presence of phosphorous in the case of the titania materials: the low degree of crystalline wall and the high surface concentration of defects lead to surface electron-hole recombination, and/or the poisoning of catalytic surface sites by the phosphorus remaining from the templates. Since high surface area phosphate-free mesoporous titania is now readily available, the presence of phosphorous in these materials should no longer hinder applications,[90] however it appears that the low crystallinity of the walls of the structure may be the tallest hurdle to overcome before the development of functional mesoporous titanium oxide photocatalysts can be realized.[91]

---

* This Chapter is based on the publication - reference 99.

Although mesoporous Ti oxide has been disappointing as a photocatalyst, Takahara and Domen reported more promising activity for mesoporous Ta oxide in the photocatalytic decomposition of water.[40] When as-synthesized tantalum oxide, prepared by the method of Antonelli and Ying, [32] was used as a photocatalyst, H_2 evolved in a rate of 50μmol/h. In contrast, a sample calcined at 600K after template removal by acid treatment and solvent extraction showed higher photocatalytic activity and released both H_2 and O_2 in a stoichiometric ratio, even though a brief induction period was observed. The initial H_2 evolution was attributed to the decomposition reaction of the remaining surfactants and the stoichiometric evolution of H_2 and O_2 started after complete consumption of the surfactant template. A NiO loaded sample showed higher photocatalytic activity and shorter induction time than those samples without NiO since NiO can act as co-catalyst in the water decomposition reaction. The optimal NiO loading level for the overall water decomposition was found to be 4.0wt%. The NiO loaded samples showed an important trend in increasing photocatalytic activity. Thus, mesoporous Ta_2O_5 showed better photocatalytic activity than the bulk amorphous and crystallized samples due to its higher surface area. These high activities as compared to those reported above for titania and niobia were explained by the different band gaps of the respective materials. The authors suggest that mesoporous Ta oxide functions as an efficient photocatalyst in this case [40] because the very thin walls of the structure ensure that virtually all electron-hole pairs generated are close enough to the surface to allow rapid migration and reaction with water.

As mentioned in Chapter 1 that mesoporous Ta oxide, when treated with bis(toluene) titanium, converts dinitrogen to ammonia on the surface.[78] This is important because it demonstrates that the Ti-reduced surface of the Ta oxide mesostructure can split dinitrogen, the first part of the Schrauzer process, and this reduced species can react with ambient moisture to form ammonia. Further, the activity of mesoporous Ta oxide as a photocatalyst in water splitting, suggests it may also be useful in the Schrauzer process. The use of a Ta oxide surface is also of special interest due to recent work by Fryzuk[57] demonstrating that organometallic Ta hydrides are capable of coordinating and partially reducing dinitrogen. In this chapter we focus on the photocatalytic behavior of pure mesoporous tantalum oxide, Fe^{3+} doped tantalum oxide, and semiconducting bis(toluene) titanium reduced mesoporous tantalum oxide. Fe was used in this system because both Schrauzer [86] and Palmisano [87] showed that Fe was the best dopant for the photocatalysis in the case of titanium oxide and also because Fe species are important as active centers in the commercial Haber process. Furthermore, X-ray studies on biological nitrogen fixation have suggested that a seven-Fe cluster in Fe/Mo nitrogenase is the site of N_2 reduction.

2.1 Experimental Section

2.1.1 Chemical and Catalyst Preparation

All chemicals, except tantalum ethoxides from Alfa Aesar, were obtained from Aldrich. Mesoporous tantalum oxides were synthesized following the ligand-assisted templating method introduced by Antonelli and Ying.[32] Fe^{3+} doped catalysts were prepared by aqueous impregnation of iron nitrate nonahydrates with mesoporous tantalum oxide for 4h with stirring and dried in oven at 110 °C overnight, then calcined in furnace at 300 °C for 3-4 h. Bis(toluene) titanium reduced catalysts were prepared by stirring 0.5g of the mesoporous solid with 0.5g of bis(toluene) titanium in 50ml of toluene. The mesoporous solid immediately turns from a light faun color to a deep blue-black. After 1 day of additional stirring to ensure complete absorption of the organometallic, the reduced material was collected by suction filtration under nitrogen and washed several times with toluene. The resulting black material was dried *in vacuo* at 10^{-3} Torr on a Schlenk line until all condensable volatile had been removed.

2.1.2 Apparatus and Procedure for Photocatalysis

All experiments were conducted in a U-shaped Pyrex reactor with a sintered glass frit as the fixed bed. A 450W UV photochemical lamp was set up parallel to the reactor at a distance of about 8cm. The photocatalytic reactions were initialized by feeding N_2 (ultrahigh purity), bubbled through deionized water at a constant flow rate of $60cm^3/min$, into the reaction tube. NH_3 produced from the reaction was absorbed by a 60ml 0.01N HCl aqueous solution, which was replaced every one hour and kept for subsequent quantitative determination by the "indophenol blue method" .[87] This method detects both NH_4^+ and NH_3 forms of N, the detection limit was reported to be about 10 μg NH_3-N/L, and Beer's law was obeyed up to about 1200 μg NH_3-N/L (Figure 1). After 3 h run, samples were flushed again by pure helium to measure the adsorbed NH_3 on the powder surface. However, complete release of trapped NH_3 may require heating at 573K or higher for several hours. Comparison experiments were also conducted under same operation conditions but using inert helium instead of the mixture of N_2+H_2O as the

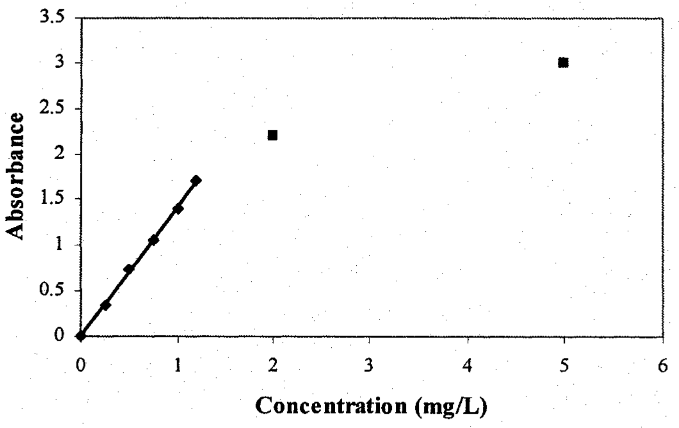

Figure 13. Standard curve of absorbance versus concentration for indephenol blue method.

feeding gas. These experiment are important for the $Fe(NO_3)_3$ doped catalysts in order to eliminate trace amount of ammonia formed by heat treatment of the surface nitrate.

2.1.3 Characterization

Nitrogen adsorption and desorption data were collected on a Micromeritics ASAP 2010. X-ray diffraction (XRD) patterns (Cu Kα) were recorded on a Bruker AXS D8-Discover diffractometer with a 2D GADDS detector. All X-ray photoelectron spectroscopy (XPS) peaks were referenced to the carbon C-(C, H) peak at 284.8 eV and the data were obtained using a Physical Electronics PHI-5500 using charge neutralization. Transmission Electron Microscopy (TEM) pictures were obtained by using a H9000 HR-TEM operated at 300 kV. The powder was deposited on a SiO_2 coated Cu grid.

2.1.4 Stock Reagents for Indophenol Blue Method

1) Phenol-alcohol reagent: dissolve 5g of phenol (C_6H_5OH, 99+%, A.C. S reagent) in 95% ethyl alcohol to a final volume of 50 ml.

2) Sodium nitroferricyanide(III) dehydrate(nitroprusside)($Na_2Fe(CN)_5NO.2H_2O$, 99%, A.C.S reagent): dissolve 0.25g in deionized water to a final volume of 50 ml. Store in dark bottle for not more than 1 month.

3) Alkaline complexing reagent: dissolve 20g of sodium citrate dehydrate ($HOC(CO_2Na)(CH_2CO_2Na)_2.2H_2O$, 99+%, A.C.S reagent) and 1 g of sodium hydroxide in DI water to a final volume of 100 ml.

4) Sodium hypochlorite (NaOCl, available chlorine $\geq 5\%$): use commercial bleach, as new as possible

5) Oxidizing solution: add 20 ml alkaline solution (3) to 5 ml sodium hypochlorite (4). Prepare fresh daily.

2. 2 Results and Discussion

2.2.1 Pure Mesoporous Tantalum Oxide

The X-ray diffraction patterns for a sample of mesoporous tantalum oxide, and that of the material treated in oven at 300°C for 3 h are shown in Figure 14. The intense (100) reflection at d=2.7 nm without resolved (110) and (200) reflections, is consistent with a wormhole structure rather than a highly ordered hexagonal structure. Apart from a slight broadening and diminishing in intensity, the XRD pattern of the calcined material shows little difference from that of the starting material, demonstrating that the initial mesostructure is largely retained after heat treatment. Figure 15 shows the nitrogen adsorption and desorption isotherms of these materials. Heat treatment results in a decrease in specific Brunauer-Emmett-Teller (BET) surface area from 624m^2/g to 366m^2/g and a corresponding decrease in the cumulative Horvath-Kowazoe (HK) pore volume from 0.304cm^3/g to 0.103cm^3/g, with the pore size remaining at 23 Å. Unlike

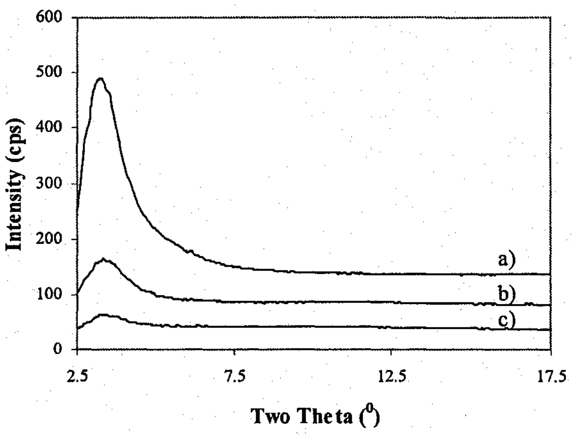

Figure 14. X-ray powder diffraction patterns for (a) mesoporous Ta oxide (S1), b)mesoporous Ta oxide after calcination at 300°C for 3h (S7), and c) 1% Fe^{3+}-doped mesoporous Ta oxide after calcination at 300°C for 3h (S8).

MCM-41, which has a sharp pore size distribution and a typical type IV isotherm, these materials possess a broader pore size distribution and an isotherm somewhere between that of type I and IV due to the pore size, which is on the cusp between the microporous

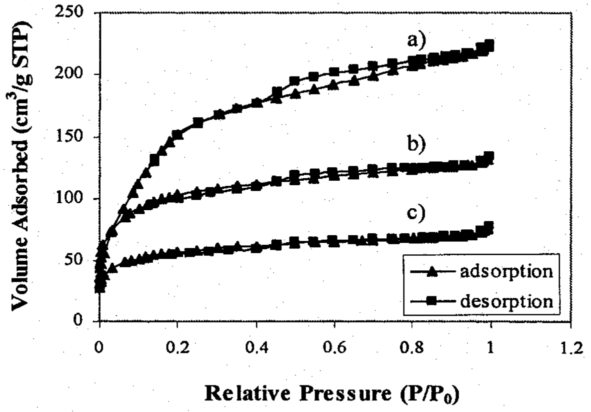

Figure 15. Nitrogen adsorption-desorption isotherms for (a) mesoporous Ta oxide (S1), (b)mesoporous Ta oxide after calcination at 300 °C for 3h (S7), and c) 1% Fe^{3+}-doped mesoporous Ta oxide after calcination at 300°C for 3h (S8).

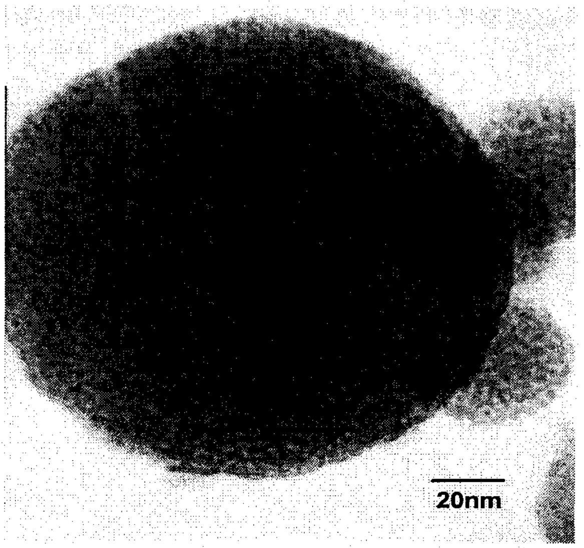

Figure 16. TEM of pure mesoporous Ta oxide (S1).

and mesoporous regimes. TEM was used to directly image mesoscopic order, particle morphology, as well as pore size and wall thickness of this material. Figure 16 clearly shows spherical particles with a wormhole pore structure consistent with XRD pattern; the measured pore size is about 25 Å, in good agreement with the results from nitrogen adsorption; the wall is roughly 15 Å, differing slightly from the calculated value of 8Å on the basis of d spacing and HK pore size assuming a perfectly hexagonal unit cell.

Photocatalytic activities of pure Ta oxide (S1) and Ta oxide after heat treatment (S2, S7) are listed in Table 1. Pure tantalum oxide without any treatment only shows low activity of 0.263μmol/g/h and thermal treatment at 300°C for 3h (S7) improves the activity to 0.683μmol/g/h. Prolonged heating time decreases the activity again to 0.47μmol/g/h (S2). In order to examine the oxidation states of surface Ta and possible N species in these materials, XPS measurements were carried out. Figure 17 shows the Ta 4f $_{5/2,\ 7/2}$ region for pure mesoporous Ta oxide before and after the photocatalytic reaction.

Table 4. Effects of thermal pretreatment and Fe^{3+} doping on photocatalytic activity.

Sample	Catalyst Composition and Pretreatment Conditions	BET Surface Area (m^2/g)	Average Activity (over 3h) (μmol/g/h)
S1	Pure Ta oxide without any treatment	624	0.263
S2	Pure Ta oxide, fired at 300 °C for 4h	319	0.47
S3	0.3% Fe^{3+}-doped Ta oxide, 300 °C for 4h	225	0.312
S4	0.5% Fe^{3+}-doped Ta oxide, 300 °C for 4h	199	0.739
S5	1% Fe^{3+}-doped Ta oxide, 300 °C for 4h	196	0.79
S6	2% Fe^{3+}-doped Ta oxide, 300 °C for 4h	196	0.35
S7	Pure Ta oxide, fired at 300 °C for 3h	366	0.683
S8	1% Fe^{3+}-doped Ta oxide, 300 °C for 3h	199	0.794
S9	Pure Ta oxide, fired at 300 °C for 3h, then reduced with bis(toluene) titanium	293	0.702

The emissions at 26.6eV and 28.5eV are characteristic of Ta (V) and demonstrate that there has been little or no change in the oxidation state of the Ta over the course of the reaction. The N 1s region of this spectrum before and after photocatalytic run are also similar (Figure 18), showing a single peak at 405 eV for the Ta 4p $_{3/2}$ emission. The expected N 1s emission for ammonia or other nitrogen species (396-403 eV) are not seen either because the Ta emission is too large and obscures the N emission, or because the quantities of N on the surface after the reaction are too small to be detected by XPS.

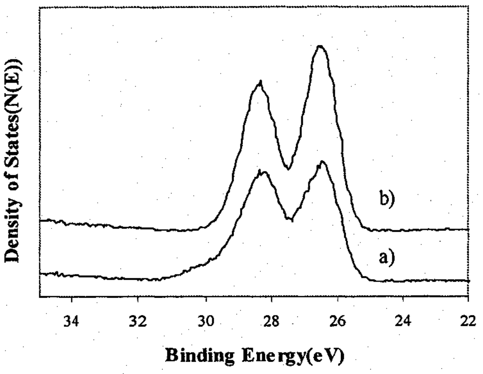

Figure 17. XPS spectra of the Ta 4f region for S7 (a) before photocatalytic reaction, and (b) after a 3 h photocatalytic reaction.

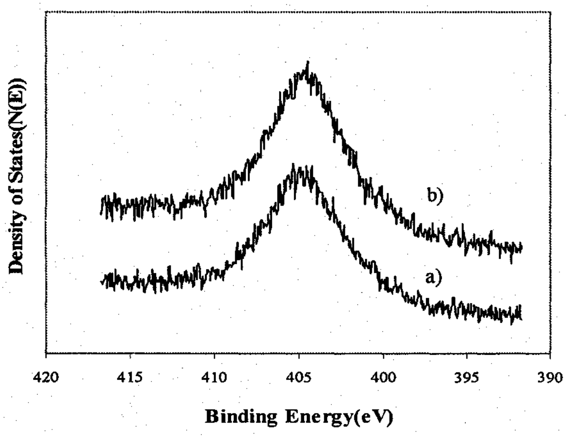

Figure 18. XPS spectra of the N 1s region for S7 (a) before photocatalytic reaction, and (b) after a 3 h photocatalytic reaction.

The improved activity on heat treatment is not unexpected, because it increases local crystallization of materials, which often leads to more efficient migration of electrons and holes through the lattice to the surface. In Schrauzer's work, [86] conversion from the anatase phase to the rutile modification by heat treatment at 1000°C was a prerequisite for high activity. In contrast, mesoporous tantalum oxide is considerably photoactive without heat treatment, as Domen reported, [40] most probably because of the small wall thickness, which enables the excited electron to migrate to the surface. While heat treatment in the case of the mesoporous Ta oxides initially improves the activity, prolonged calcination causes a diminution of active surface in addition to an increasing loss of surface metal hydroxide groups, both contributing to a decrease of photocatalytic activity. In the case of very high surface mesoporous materials, this problem becomes even more prominent because of the apparent incompatibility of the presence of the mesostructure and the crystallinity of the walls. All mesoporous materials reported so far have either amorphous wall structures or disconnected nanocrystalline grains embedded in the walls. Crystallization of the walls to bulk oxides occurs upon exhaustive thermal treatment, resulting in a collapse of the mesostructure. Thus high surface area and porosity is normally offset by crystallinity. In light of these observations, the difference of activity between S2 and S7 likely results from their different surface area.

2.2.2 Fe^{3+} Doped Mesoporous Tantalum Oxides

To obtain higher activities, we prepared a series of Fe^{3+} doped Ta oxides with different loading levels. The XRD pattern and the N_2 adsorption and desorption isotherm of 1 wt% Fe^{3+} doped sample are also shown in Figures 14 and 15, respectively. Surprisingly, the BET surface area of this sample decreased by more than two-thirds, i.e. from original 624m^2/g to 199m^2/g, although the HK pore size remains unchanged. After carefully examining each step of preparation, we found the loss in surface area originates mainly from the aqueous impregnation of $Fe(NO_3)_3$. This phenomena is not uncommon as[75, 92] the Davis group reported that Ru/MCM-41, when impregnated with $CsNO_3$ in aqueous solution, experiences a loss of surface area to 623 m^2/g from 1058m^2/g and a loss of total pore volume to 0.417cm^3/g from 1.015cm^3/g. This effect is likely related to the surface tension of water confined in the nanopores. Liquid water has a much higher surface tension (72.75×10^{-3} N.m^{-1} at 20°C) than organic solvents (23.7×10^{-3} N.m^{-1} for acetone, at 20°C).

XPS spectra of Fe^{3+} doped tantalum oxides for Ta 4f and N 1s regions are quite similar to those of pure mesoporous tantalum oxides, except that the two peaks of Ta 4f $_{5/2,\ 7/2}$ show slight broadening and relatively weaker in intensity, which can be attributed to a broader distribution of Ta sites in the walls of the material. The Fe 2p region in all materials could not be resolved due to the very low content of this element.

The activities of all Fe^{3+} doped catalysts from experiments are listed in Table 4. Clearly, the highest activities appear on the 1 wt% Fe^{3+} doped samples, S5 and S8. Although the underlying reason for this Fe-induced enhancement of activity is not completely clear, it may be related to a modification of the band-gap region and/or formation of a permanent space charge region in the walls. Fe has always been one of the best choices for the photocatalytic conversion of dinitrogen to ammonia.[87] For example, Palmisano et al.[87] demonstrated that the pure TiO_2, with band-gap energy in the near UV, is not active under visible light, but doping with Fe extends the light absorbed by TiO_2 to the visible region. An optimal doping is achieved when a space charge region exists with electric force more than 0.2eV, whose thickness is more or less equal to the light penetration depth which ensures all the generated electron-hole pairs efficiently separated. Tantalum oxides possess a band-gap energy of 4.0 eV and absorb in near UV without doping, so that the modification of bang-gap region should not be necessary. In fact, pure tantalum oxide (S7) demonstrates moderate photocatalytic activity, while the activity of the 0.3% Fe^{3+} doped sample(S3) is actually lower than that of pure tantalum oxide (S2, S7). However this surprising observation can be rationalized when considering the additional and offsetting effect of the loss of surface area resulting from aqueous impregnation.

The nearly identical activities of S5 and S8 are also of some interest. From the standpoint of surface area alone, S8 should have higher activity than S5. After careful examination of the experimental data presented in Figure 19 and 20, it becomes evident that S5 has more pre-adsorbed NH_3 than S8 although they have theoretically the same wt % $Fe(NO_3)_3$ doping content. This suggests that more catalytically active Fe is present in S5 than in S8, possibly due to the longer calcination time. Since we cannot identify the exact phase(s) of Fe(III) from XRD and XPS because of the low level of Fe, it is not possible at this stage to establish any structure property relationships that might elucidate the nature of the active Fe centers. The higher content of more active Fe in S5 counteracts the disadvantage of lower surface area, bringing the two samples to the same level of activity.

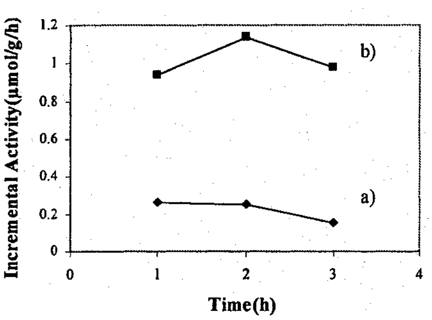

Figure 19. Comparison experiments on S8 under UV lamp, (a) Helium is the only feeding gas, and (b) a mixture of N_2+H_2O is the feeding gas.

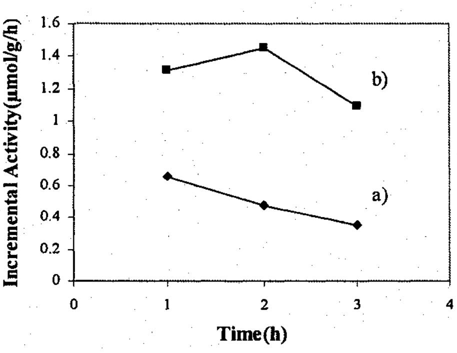

Figure 20. Comparison experiments on S5 under UV lamp, (a) Helium is the only feeding gas, and (b) a mixture of N_2+H_2O is the feeding gas.

2.2.3 Mesoporous Ta Oxide Reduced with Bis (toluene) Titanium

To improve the activities of these catalysts by improving electron-hole separation on the surface of the Ta oxide mesostructure, we pursued methods of improving surface conductivity in these otherwise insulating structures. The development of a stoichiometric process for fixing dinitrogen on the surface of a mesoporous oxide reduced with bis(toluene) metal species[76,77] was an extension of previous work in which organometallic sandwich compounds were used as reducing agents to make low-dimensional molecular conductors in the pores of the mesostructure.[93-97] The introduction of organometallic into the pores was similar to a classical redox intercalation reaction in which an electron donor reduces the walls of the inorganic host to create a material with periodic charge regions consisting of anionic metal oxide phase and a cationic dopant intercalate phase. In the case of bis(toluene) titanium and mesoporous Ta oxide, the organometallic acts as a reductant, but does not retain its structural integrity on loss of electrons, instead losing the toluene ligands to essentially deposit Ti atoms on the surface of the mesostructure while also reducing the mesostructure. XPS studies show that there are several Ta and Ti environments in this material, including a low valent Ti species that reacts almost spontaneously with dinitrogen to create surface nitride.[78] Charge balancing of this highly reduced mesoporous system requires that the electron-depleted low valent coat have a cationic charge and the partially-reduced higher valent coat have a negative charge. This morphology should create a depletion zone between the two layers similar to that between a p-n junction, which may be useful in promoting electron-hole separation in a photocatalytic process involving dinitrogen, since coating of n-doped titania with a p-doped conducting polymer creates a p-n junction with a depletion region that improves the thermodynamics of nitrogen reduction by water.[88] By analogy, the bis(toluene) Ti-reduced mesoporous Ta oxide may thus show very high activity towards dinitrogen in photocatalysis. These reduced materials are metallic or semiconductors depending on the degree of reduction, while other reduced mesoporous oxides are insulators. The highly conducting nature has been attributed to the low-valent coat on the surface and implies that the surface states are continuous in nature. This may provide a further advantage in photocatalysis, as surface defects and localized electron traps have been indicated as reasons why amorphous oxides usually have poor electron-hole separation properties.[41] Thus, the modification of mesoporous Ta oxide with bis(toluene) titanium to create a metallic oxide coat on the surface of the material may represent a strategy of overcoming electron localization leading to electron-hole pair recombination, since electrons tend to drift towards metallic regions on the surfaces of photocatalysts and these reduced mesoporous oxides must have a more continuous band structure with fewer surface defects in order to display such high conductivities.

Surprisingly, our catalytic runs with the bis(toluene) Ti reduced mesoporous Ta oxide catalyst didn't give much better results than pure tantalum oxide (see Table 4, S7 vs S9). The most likely explanation for this is that although bis (toluene) titanium increases the surface conductivity and creates sites capable of splitting dinitrogen, this surface coat is very air sensitive and possibly degrades as O_2 is formed over the course of the reaction. For this reason, it may be more effective to coat the inner surface of the material with a more robust semiconducting polymer in order to create an internal p-n junction capable of effecting superior electron-hole separation without degrading during the catalytic process. Since uniformly coating the inside of mesoporous materials without clogging the pores is not trivial, requiring careful selection of catalyst dopants on the inner surface and control of polymer substrate concentrations, this strategy represents the body of an independent study.

2.3 Conclusion

For the first time, the photocatalytic conversion of dinitrogen to ammonia over a mesoporous Ta oxide based catalyst was studied. All catalysts studied showed low to moderate activity and the 1 wt % Fe doped catalysts show comparable molar activities to Schrauzer's initial results. Higher surface area, heat treatment, and Fe content were found to increase the activities; however the latter two factors have an adverse effect on the first, i.e. surface area, such that optimization is hindered. Treatment of the material with bis(toluene) Ti had little effect on the photocatalytic activity, most likely due to the oxygen sensitivity of this material.

Chapter 3. Electroactive Mesoporous Tantalum Oxide Catalysts for Nitrogen Activation and Ammonia Synthesis

After decades of intense research, the activation of dinitrogen by transition metals and their compounds is still one of the frontiers of inorganic chemistry. [45-47, 53, 88, 89] The Haber-Bosch ammonia synthesis is one of the most widely used catalytic processes in industry, however the selective functionalization of dinitrogen and its use as a feedstock in the synthesis of nitrogen-containing organics has remained a challenge. Extensive research in the field of organometallic chemistry has shown that low valent early transition metal complexes can either stoichiometrically, [50, 52] or catalytically [54] cleave dinitrogen as long as the ligand environment around the metal is bulky enough to stabilize the coordinatively unsaturated metal center while still allowing access to the active site. [55] The main challenge in the selective functionalization of dinitrogen is to couple a strong enough reductant and an electrophile in the same system, while also preventing the electrophile from quenching the reductant before it can attack the more inert dinitrogen molecule. Previous studies showed that mesoporous Ti, Nb and Ta oxides, when treated with bis (toluene) Ti/Nb, form ammonia spontaneously on exposure to dinitrogen and incipient moisture, [76-78, 96, 98] suggesting that the only barrier to making this process catalytic was the re-reduction of the active site. Since it is not practical to use bis (toluene) Ti as a reductant, we began to investigate other ways of making this process catalytic. Because mesoporous Ta oxide is more thermally stable than its Nb and Ti counterparts and reduced Ta species have been implicated in both molecular-based [57] and photocatalytic [99] nitrogen activation, we chose this metal as our catalyst support. Since

Ru has been used effectively in a wide variety of Haber systems, [72, 75, 92, 100] we focused our studies on a series of Ru-doped mesoporous Ta oxides. The entire catalytic process in this case takes place on the Ru clusters in these systems, with the electrochemically inert main-group oxide support and promoter thought to modify the dispersion and electronic properties of the metal grains. In a mesoporous Ta oxide-based system there is the added possibility that dinitrogen cleavage could take place at a reduced Ta center, with the precious metal dopant functioning as a hydrogenation catalyst to regenerate the low-valent Ta sites. Hydrogen in this case would continuously form reduced Ta sites while also supplying a source of protons, thus avoiding the use of bis (toluene) Ti as a reductant and water as the electrophile. Because hydrogen is a strong enough reductant to reduce Ta (V) to Ta (II) under the right conditions, it may be expected that such a catalyst could have several oxidation states of Ta involved and that this would further influence the behavior of the system as compared to Ru supported on main-group oxides, which do not possess variable oxidation states. In order to make meaningful comparisons between our Ru-doped mesoporous Ta oxide catalyst and previously studied Haber systems, we followed a procedure directly analogous to that used to prepare and activate both Ru-MCM-41[75] and Ru-MgO catalysts, [100] employing $Ru_3(CO)_{12}$ as a Ru source and barium nitrate as the promoter.

3.1 Experimental Section

In a general procedure, a batch of 5 wt% ruthenium-doped tantalum oxide catalysts were prepared by impregnating mesoporous Ta oxide (2g, synthesized according to ref.32) with $Ru_3(CO)_{12}$ (0.22g, Aldrich) in tetrahydrofuran (THF). After stirring overnight, the mixture was evaporated in a rotary evaporator and dried *in situ* at 70°C for

4h. The yellow powders were then moved to a reaction tube and evacuated at 300°C for 3h. The temperature ramping time was 60 minutes.

To obtain the barium-promoted ruthenium catalyst with the molar ratio of Ba:Ru=1:1, the thermally decomposed 5% Ru-Ta oxide(0.5g) was stirred in a solution of $Ba(NO_3)_2$ (0.065g, Aldrich) and solvent (H_2O: EtOH=50:50; 20ml) for 4h and subsequently dried in oven at 120°C overnight. The grey powders were then moved to a U-shaped Pyrex reactor with a sintered glass frit as the fixed bed, and further dried at 100°C *in vacuo* overnight. Ultra-High-Purity (99.999%) H_2 and low oxygen (99.999%) N_2 were used as synthesis gases. To determine the activities at low temperatures ($\leq$ 250°C), the catalysts were first activated by H_2 at 350°C for 4h, then pumped in Schlenk line (10^{-3} torr) at 300°C for 2h to remove any residual surface ammonia. After cooling to reaction temperature in vacuum, a mixture of H_2+N_2 (3:1) was immediately fed into the reactor. The NH_3 produced was adsorbed by 0.01N HCl aqueous solution and analyzed by the indophenol blue method. [99] The activities at 350°C were determined in a stream of synthesis gas from the beginning.

XRD patterns (Cu Kα) were recorded on a Bruker AXS D8-Discover diffractometer with a 2D GADDS detector. XPS data were obtained on a Physical Electronics PHI-5500 using charge neutralization and all peaks were referenced to the carbon C-(C, H) peak at 284.8 eV. TEM picture was obtained by using a H9000 HR-TEM operated at 300 kV. Nitrogen adsorption and desorption data were collected on a Micromeritics ASAP 2010. Energy Dispersive X-ray Spectroscopy (EDS) line scans were done on a JEOL JSM-5800LV tungsten filament scanning electron microscope operating at an accelerating voltage of 15kV.

3.2 Results and Discussion

Figure 21(a) shows the X-ray powder pattern (XRD) of a sample of mesoporous Ta oxide synthesized with dodecylamine according to the method of Antonelli and Ying.[32]

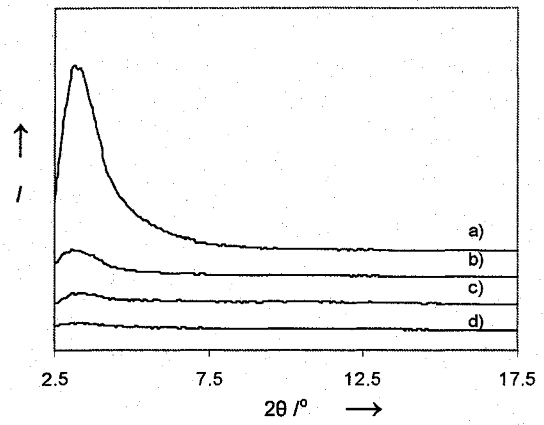

Figure 21. X-ray powder diffraction patterns for (a) mesoporous Ta oxide starting material, (b) parent catalyst Ba-Ru/Ta oxide, (c) catalyst after catalytic run at 175°C, 3h, and (d) catalyst after H_2 regeneration at 350°C, 2h.

This material possessed a BET (Brunnaur, Emmett, Teller) surface area of 541 $m^2 \bullet g^{-1}$ and an HK (Horvath Kowazoe) pore size of 23 Å. Figure 21(b) shows the XRD pattern for this same material after impregnation with 5 wt % Ru and $Ba(NO_3)_2$ at a molar ratio of Ba/Ru = 1:1. The diminished intensity suggests a loss of long range order, however the BET surface area of this material was 370 $m^2 \bullet g^{-1}$ and the HK pore size was 23 Å, indicating a retention of the overall mesoporous structure. When pure water was used for the impregnation of the Ba salt, the surface area was only 250 $m^2 \bullet g^{-1}$, possibly because damage to the pore structure caused by the higher capillary pressure of water as compared to organic solvents such as methanol. The TEM micrograph of the sample from Figure 21(a) doped with 5 wt % Ru clearly shows the disordered wormhole pore structure and

50-100 nm size of the individual grains. Higher magnification did not reveal any evidence of Ru nanoparticles, but this was not unexpected as the XRD region for metallic Ru showed no sign of distinguishable reflections. The energy dispersive X-ray (EDS) spectrum (Figure 22) of this sample did, however, provide evidence for Ru incorporation in the material. These data are consistent with the presence of Ru nanoclusters smaller than the detection threshold of XRD or TEM.

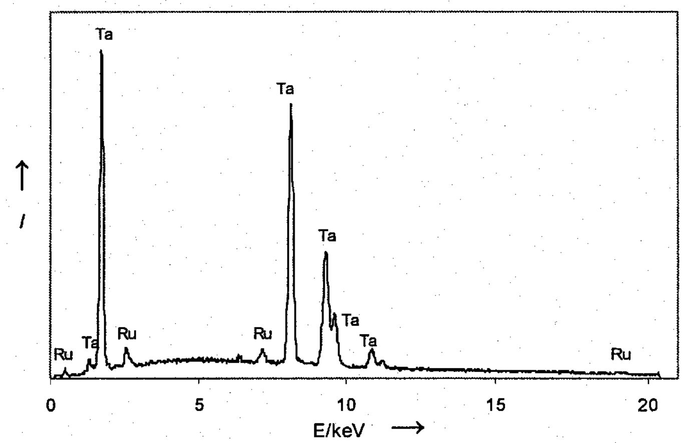

Figure 22. EDS spectrum of 5% Ru-doped mesoporous Ta oxide.

Figure 23 shows a plot of the natural log of incremental activity versus time for ammonia production by the catalyst under a stream of 1:3 $N_2 + H_2$ at 350 °C. The catalyst has a high initial activity of 163 $\times10^{-6}$ mol•g^{-1}•h^{-1} in the first hour, but then the rate drops off dramatically in the second hour and continues at a rate of 1-2 $\times10^{-6}$ mol•g^{-1}•h^{-1}. This initial rate is over 100 times greater than those reported in our mesoporous Ta oxide Schrauzer type photocatalysts, [99] and compares favorably to the values reported for alumina, silica, or magnesia supported Ru-doped MCM-41 catalysts, which fall in the range of 300 $\times10^{-6}$ mol•g^{-1}•h^{-1}.[75] Since Ta oxide (441.89 g•mol^{-1}) possesses a greater

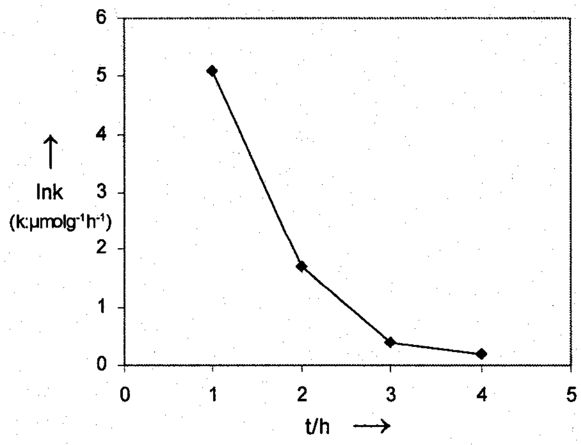

Figure 23. Natural log of incremental activity versus time at 350°C of the catalyst from Figure 21b.

molecular weight than silica (60.08 g•mol^{-1}), magnesia (40.30 g•mol^{-1}), or alumina (101.96 g•mol^{-1}), these values compare even more favorably when the activities are compared on a per-mole basis. The drop off in rate after the first hour is not understood but may be related to a combination of surface deactivation and loss of structure, as the XRD shows a further loss of mesoscopic order (Figure 21(c)) and the BET surface area drops to 229 m^{2}•g^{-1}. While some of the NH_3 formed in the initial hour may come from residual nitrate, previous studies show that N_2 is an intermediate in nitrate reduction to NH_3, and also that NH_3 is a stronger reducing agent than H_2 in reactions with NO_2, which is formed from nitrate as an initial reduction step.[102] Furthermore, $Ba(OH)_2$ also works as a promoter, although the activities are lower than the nitrate. In order to verify that the catalyst is actually producing new ammonia in the second hour and the apparent activity does not come from ammonia adsorbed to the surface in the first hour, the catalyst after 1 h of initial activity at 350 °C was placed under vacuum at 10^{-3} torr and 350 °C for 1 h before the temperature was lowered to ambient and catalysis resumed. The values obtained are from 2-5 $\times 10^{-6}$ mol•g^{-1}•h^{-1}, virtually the same as those obtained without the vacuum step. This firmly establishes that these catalysts are producing new ammonia from N_2 and H_2 under these conditions.

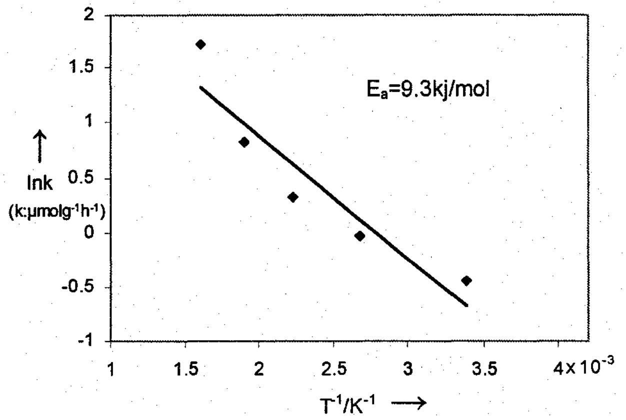

Figure 24. Arrhenius plot for the catalyst from Figure 21b.

The catalyst demonstrates only slightly lower activities in the second hour at ambient temperature than it does at 350 °C also in the second hour. This low degree of temperature dependence is somewhat surprising, as standard Ru-based Haber catalysts show a strong relationship between temperature and activity. Figure 24 shows the Arrhenius plot over a range 295 K to 623 K and the activities are listed in Table 5. Samples were first reduced by H_2 only at 350 °C for 4h and then left under vacuum for 2h at 300°C to remove any adsorbed surface species. The catalyst was then cooled to the

Table 5. Activities at different reaction temperatures.

Temperature (Kelvin)	Activity k (μmolg^{-1}, 1h)	lnk (k: μmolg^{-1}h^{-1})
295	0.64	-0.446
373	0.97	-0.03
448	1.38	0.322
523	2.28	0.824
623	5.52	1.71

reaction temperature and treated with a flow of $N_2 + H_2$ for 1h. The activation energies (Ea) calculated from this plot is 9.3 kJ•mol^{-1}, roughly 10% of that calculated for Ru-doped catalysts on other supports (Ea for Ru/BaMCM41 is 90 kJ•mol^{-1}; Ru/BaMgO is 76 kJ•mol^{-1}). This, coupled with the somewhat low activities across this temperature range, suggests a different mechanism is at work and involving a small number of active sites with a low activation barrier. This is consistent with our work on bis (toluene) Ti reduced mesoporous Ta oxides, which form ammonia from dinitrogen and moisture almost instantly at room temperature, suggesting a low activation barrier to this stoichiometric process.[78]

In order to further study the mechanism of ammonia formation, X-ray photoelectron spectroscopy (XPS) was conducted at various stages of the synthesis and catalysis. Figure 25 shows the Ta 7/2, 5/2 from the 4f region. The spectrum for the catalyst before the catalytic run is shown in (a) with emissions at 26.8 eV and 28.6 eV respectively. This compares closely with the binding energies of pure mesoporous Ta (V) oxide, which fall at 26.9 eV and 28.7 eV, respectively. The spectrum in (b) shows the 7/2, 5/2 emissions from the material in (a) after a catalytic run in $N_2 + H_2$ for 3 h at 175 °C. There is a clear broadening of these emissions with binding energies as low as 25.1 eV, indicating that several reduced surface Ta species are present. For comparison, a sample of mesoporous Ta oxide reduced with 1.0 eq. of Rb naphthalene shows a 5/2 emission centered at 26.0 eV. [103] This suggests that lower oxidation states than Ta (IV) are involved in the catalytic process. The Ru 3p region for these same samples (Figure 26) displays a commensurate shift of the Ru peaks to lower binding energy after a catalytic run, consistent with multiple reduced Ru species on the surface. Since pure mesoporous Ta oxide does not

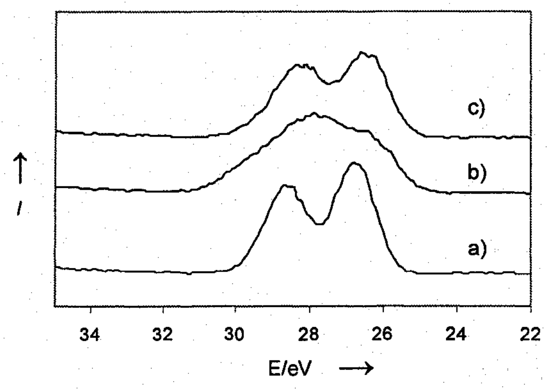

Figure 25. XPS spectra of the Ta 4f region for (a) parent catalyst Ba-Ru/Ta oxide, (b) after catalytic run at 175°C, 3h, and (c) catalyst after H_2 regeneration at 350°C, 2h.

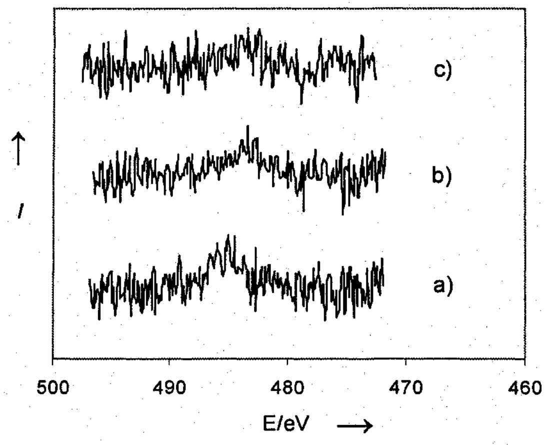

Figure 26. XPS spectra of the Ru 3p region for (a) parent catalyst Ba-Ru/Ta oxide, (b) after catalytic run at 175°C, 3h,and (c) catalyst after H_2 regeneration at 350°C, 2h.

react with H_2 under these conditions, the Ru dopant must act as an interface and lower the activation barrier to the reduction of the Ta species. Reduced Ta has been previously implicated [57, 78] in stoichiometric N_2 activation by organometallic complexes, suggesting that these Ru-doped mesoporous Ta oxide catalysts may function via a different mechanism than standard Ru-based Haber systems. The latter catalysts are somewhat structure sensitive and reaction orders in hydrogen are negative in the Ru systems, suggesting that surface coverage by hydrogen can block adsorption of dinitrogen and retard the rate. In our system it is clear from the XPS that hydrogen must at some stage provide electrons to the Ta sites and that some overspill from the Ru particles is thus involved. Figure 27 shows a representation of a possible mechanism in which electrons from H_2 are funneled through the Ru particles to the mesoporous Ta network, where they reduce certain sites (dark blue) to a form capable of attacking N_2. This mechanism would likely depend on the work function, Fermi level and degree of Ohmic contact at the metal-metal oxide interface as well as the presence of conduction pathways across the surface. Work by our group has shown that reduced mesoporous transition metal oxides can be semiconducting or metallic depending on the composition, suggesting that electron transfer across the mesoporous Ta oxide framework is indeed possible. [76-78, 96, 98] Preliminary kinetic data suggests that the rate decreases with decreased H_2 concentration, further supporting the role of low valent Ta in the process. The nature of deactivation is

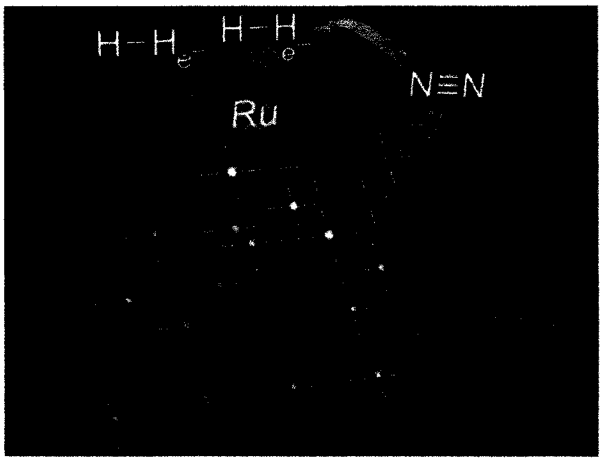

Scheme 27. Possible mechanism for ammonia formation on Ru-doped mesoporous Ta oxide materials showing reduced Ta sites in dark blue.

under investigation. The role of the Ba promoter in our system is not clear. In standard Ru-based Haber systems Aika has linked the promoter to an electronic modification of the Ru surface by the promoter to enhance electron donation into the N_2 antibonding orbital.[72] Other workers have argued against this in favor of a picture where the promoter lowers the absorption energy of ammonia on the Ru surface, thus pushing the equilibrium on the surface in favor of regenerating more ammonia after desorption.[101]

After several hours of catalytic activity, the materials were regenerated by treatment with H_2 at 350 °C for 2h. The BET surface area drops slightly to 220 $m^2 \bullet g^{-1}$ (Table 6) and the main reflection in the XRD diminishes further in intensity as shown in Figure 21(d). The binding energy in the Ru 3p region remains relatively constant to that after regeneration, but the Ta 5/2, 7/2 emissions sharpen considerably (Figure 25, trace c), indicating a change in oxidation state and diminution in the number of surface Ta species in the lowest oxidation states (ca. 25 eV). The activities of the catalyst after regeneration drop to around $2 \times 10^{-6} mol \bullet h^{-1} \bullet g^{-1}$. These data are consistent with a loss of active sites from some surface deactivation process, and demonstrate that hydrogen treatment does not completely regenerate the catalyst. This also suggests that the active sites may be related to the emissions at ca. 25 eV, which correspond to small amounts of Ta in very low oxidation states. This is fully consistent with the Arrhenius data and observations

Table 6. Surface areas of catalyst from Figure 24 after subsequent steps in the catalytic process.

No.	Catalyst processing conditions	BET surface area (m^2g^{-1})
1	Mesoporous Ta oxide starting material	541
2	5% $Ru_3(CO)_{12}$-doped Ta oxide after decomposition *in vacuo* at 300°C, 3h	470
3	Parent catalyst Ba-Ru/Ta, Ru=5 wt %, Ba/Ru=1	370
4	Parent catalyst after H_2 reduction at 350°C, 4h	242
5	Material from 4 after vacuum treatment at 300°C, 2h	237
6	Material from 5 after catalytic run at 175°C, 3h	229
7	Material from 6 after H_2 regeneration at 350°C, 2h	220

from organometallic chemistry involving the role of low valent early transition metals in nitrogen activation. Since the XPS clearly indicates the role of reduced Ta in the catalytic process, the inefficient regeneration by hydrogen may be related to an increased barrier to electron transfer on the surface after a catalytic run, or a change in local coordination geometries of the active site after prolonged heating.

3.3 Conclusion

In summary, mesoporous Ta oxide doped with Ru and Ba is an active catalyst for conversion of N_2 and H_2 into ammonia. Initial activities are high, but drop and stabilize after the first hour and continue for several hours, even at room temperature. The Arrhenius plot and XPS data suggest a different mechanism than standard Ru-doped Haber catalysts, where the precious metal acts as an electrode interface to reduce surface Ta sites, which are then able to attack N_2. This system thus takes advantage of the well-documented propensity for low-valent early transition metals to attack dinitrogen, while also avoiding exotic electron feedstocks or aggressive electrophiles, often required in these systems. The mild temperatures under which the catalyst operates may open the door for new reactions involving nitrogen incorporation into organics, most of which cannot survive the high operating conditions of standard Haber systems. Further studies on kinetics and use of different metal dopants and promoters are required to better understand the nature of the active site and improve activity and longevity of the catalyst.

Chapter 4. Support and Promoter Effect of Ru-based Mesorporous Ta Oxide Catalysts for Ammonia Synthesis

The activation of dinitrogen has been one of the holy grails of inorganic chemistry for several decades. [53, 104] A recent resurgence of interest precipitated by several advances in organometallic [46, 50, 52, 54, 55] and materials chemistry [75, 88, 100] only reconfirm the importance of this reaction. While the synthesis of ammonia using transition metal catalysts is one of the most important catalytic processes in all of chemistry, the use of dinitrogen as a feedstock for the synthesis of fine organics under mild conditions has still remained elusive. Thus, the discovery of new and milder ways of selectively cleaving and functionalizing the N-N triple bond is one of the great challenges of modern inorganic chemistry. Over the years various supported transition metal-based catalytic systems have been studied for ammonia synthesis. [63, 70-75, 100] For this particular process Ru is generally accepted to be superior to Fe or other transition metals, so most current efforts have focused on investigating the effects of different supports and promoters. Common supports include main group oxides such as magnesia, alumina, and silica, while the promoters are usually alkali metals, alkali metal oxides/hydroxides, and alkali earth metals oxides because of their strong electron donating abilities, which are believed to modify the reactivity of the active Ru center. [72] Electronegativities of these promoters have been used as a rough criterion to evaluate their mechanism of promotion, which often correlates well with the rate of ammonia production, however this is not always the case.[74, 75, 100] Alkali metals are good electron donors, however these metals are quite sensitive to oxygen-containing compounds such as water and dioxygen, consequently are turned into oxides or hydroxides. Because of this concern, oxide promoters might be more practical than the metal analogs although the promotion effects are somewhat lower. [67] In Chapter 3, a new Ru-doped mesoporous Ta oxide catalytic system was established which can convert dinitrogen into ammonia over the temperature range of 295K to 623K.[105] This system was an extension of work we conducted on bis(toluene) Ti reduced mesoporous Ta oxides which demonstrated that metallic phases on the surface of the mesostructure are capable of stoichiometrically cleaving the N-N triple bond of dinitrogen at room temperature [78] and then producing ammonia as long as ambient moisture was present. Since bis(arene) complexes constitute an exotic and expensive source of electrons in any catalytic process, we developed a new Ru-doped mesoporous Ta oxide system which uses H_2 as a source of electrons and protons in the sequential reduction of dinitrogen. This system thus represents a marriage of state-of-the-art Haber catalysis with strategies developed from our electroactive bis(arene) reduced mesoporous transition metal oxides. The fundamental difference between this new system and the more traditional Haber systems is that the mesoporous framework has a capacity for variable oxidation states which magnesia, alumina, and silica do not possess. This opens the doorway for the involvement of reduced Ta in the process, which is particularly intriguing given that Fryzuk has found that low-valent Ta complexes readily activate dinitrogen under mild conditions. [52] The activities of this new Ta-based system are unusual, exhibiting high initial activity which rapidly drops off after the first hour. Arrhenius plots provide surprising activation energies of only 9.3 kJ/mol, roughly 10% that reported for the traditional Ru-based Haber systems. XPS studies on the material during several stages of the process show strong evidence for involvement of reduced Ta species. These data suggest a new mechanism, in which the Ru acts as an interface to transfer electron density from hydrogen to neighboring Ta sites on the oxide support, which in the reduced form are then able to cleave dinitrogen. In order to better understand this new system, the dependence of activity on type of promoter, promoter precursor, Ru precursor, promoter and Ru loading levels, as well as hydrogen activation temperature has been performed.

4.1 Experimental Section

4.1.1 Materials and Equipment

All chemicals unless otherwise stated were obtained from Aldrich. All experiments were conducted in a U-shaped Pyrex reactor with a sintered glass frit as the fixed bed. NH_3 produced from the reaction was absorbed by 0.01N HCl aqueous solution, and quantitatively determined by the "indophenol blue method". [99] TEM images were obtained by using a H9000 HR-TEM operated at 300 kV. Nitrogen adsorption and desorption data and BET surface area were collected on a Micromeritics ASAP 2010. H_2-TDA measurements were performed on a TGA/SDTA851 (Mettler Toledo) over the temperature range from room temperature to 450°C at a heating rate of 2°C/min, in a stream of 96% argon and 4% hydrogen with a flowing rate of 30 cm^3/min.

4.1.2 Synthesis

(a) Mesoporous Ta oxide: Mesoporous tantalum oxides were synthesized following the ligand-assisted templating method introduced by Antonelli and Ying. [32]

(b) Ru-doped mesoporous Ta oxide: In a general procedure, 5 wt% ruthenium-doped tantalum oxide catalyst was prepared by impregnation mesoporous Ta oxide with $Ru_3(CO)_{12}$(99%) in tetrahydrofuran (THF). After stirring overnight, the mixture was evaporated in a rotary evaporator and dried in situ at 70°C for 4h. The yellow powders were then moved to a reaction tube and evacuated at 573K for 3h. The temperature ramping time was 60 minutes. When ruthenium chloride hydrate ($RuCl_3.xH_2O$, 99.98%) was used as ruthenium precursor, $RuCl_3.xH_2O$ was impregnated with mesoporous Ta oxide in methanol. After stirring overnight, the organic solvent was removed in a solvent storage flask on a Schlenk line.

(c) Nitrates ($Ba(NO_3)_2$, $CsNO_3$ and $La(NO_3)_3$) promoted Ru/Ta oxide catalysts: To obtain the nitrate promoted catalyst, typically 0.5g Ru-Ta oxide was stirring in a solution of nitrates ($Ba(NO_3)_2$, Alfa Aesar, 99.95%, metals basis; $CsNO_3$, 99%; $La(NO_3)_3.xH_2O$, 99.9%) and solvent (H_2O: EtOH=50:50) for 4h and subsequently dried in oven at 120°C overnight. The powders were then moved to a U-shaped Pyrex reactor with a sintered glass frit as the fixed bed, and further dried at 373K *in vacuo* overnight.

(d) $Ba(OH)_2$ and Barium isopropoxide promoted Ru/Ta oxide catalysts: Considering that both Ba precursors, when exposed to CO_2 in air, might be converted to $Ba(CO_3)_2$, and lose their promoter activity, barium hydroxide ($Ba(OH)_2$, tech. ~95%) was impregnated with as-synthesized Ru/Ta in methanol in Argon glove box, after stirring 4 h, the solvent was removed in an air-free solvent storage flask on a Schlenk line at 100C; Barium isopropoxide ($Ba[OCH(CH_3)_2]_2$, Alfa Aesar, 20% w/v in isopropanol, density 0.89) analog was impregnated with Ru/Ta in isopropanol, and the solvent was then removed by the same manner.

4.2 Results and Discussion

4.2.1. Characterization

Since heterogeneous catalyst for ammonia synthesis typically exhibit complicated multi-component behavior in which the support, the precious metal dopant, and the promoter all play an important role, we undertook a series of compositional studies in order to establish important trends which may shed light on the reaction mechanism. In these studies XRD and TEM was used to confirm the mesostructure of all catalysts. The TEM image in Figure 28 clearly shows the disordered wormhole pore structure and 50-100 nm size of the individual mesoporous particles, however individual Ru metal grains could not be located within the pores. This was not unexpected, as XRD did not show any reflections for Ru metal. However, energy dispersive X-ray spectroscopy (EDS) and XPS provided firm evidence for the presence of metallic Ru in the materials. [105] This indicates that Ru is finely distributed on the material surface, and the grain size is below the detection limit of TEM or XRD. Figure 29 shows the nitrogen adsorption-desorption isotherms of the mesorporous Ta oxide starting material, the Ba-Ru/Ta catalyst before H_2 reduction, and this same catalyst after H_2 reduction. Hydrogen heat treatment at 350°C for 4h results in a decrease in specific BET surface are from 541m^2/g to 242m^2/g, and a corresponding decrease in the cumulative Horvath-Kowazoe (HK) volume from

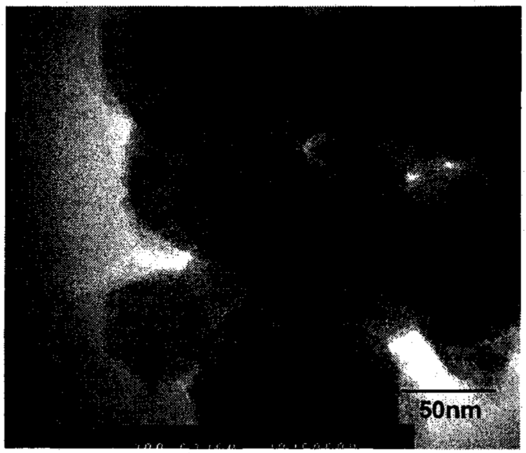

Figure 28. TEM of 5% Ru-doped mesoporous Ta oxide.

$0.282 cm^3/g$ to $0.092 cm^3/g$, with the pore size remaining at 23.3 Å. The nitrogen adsorption-desorption isotherms show characteristics of both type I (for microporous) and type IV (for mesoporous) because of a broader pore-size distribution and the pore size on the cusp between the microporous (d <20 Å) and mesoporous (20 Å <d<500 Å) regimes.[20] This behavior is typical of C_{12}-templated mesoporous Nb, Ta, and Ti oxides studied in our group. The HK pore-size distribution shows a major peak at 23.3 Å, demonstrating that the doping process has not compromised the narrow pore size distribution of the parent mesostructure.

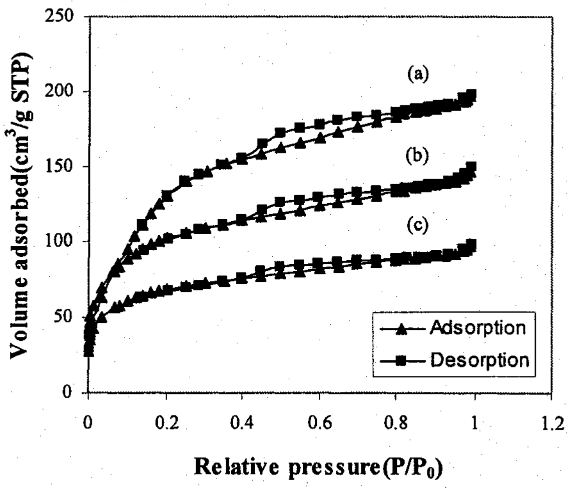

Figure 29. Nitrogen adsorption-desorption isotherms for (a) pure mesoporous Ta oxide, (b) catalyst Ba-Ru/Ta (Ru=5wt%, molar ratio Ba/Ru=1) before H_2 activation, and (c) catalyst from (b) after H_2 activation at 350°C for 4h, followed by catalytic run at 175°C.

4.2.2 Effect of Reduction Temperature

The rate of ammonia synthesis was measured over Ru/Ta oxide catalysts promoted with $Ba(NO_3)_2$ and $CsNO_3$ and the effect of reduction temperature was studied. The Ru precursor used for these studies was $Ru_3(CO)_{12}$ because this precursor proved to be the most effective in our previous studies and has also been used successfully in mesoporous silica-based Haber systems. The activity of Ru-doped mesoporous Ta oxide catalysts decreases for both promoters when the reduction temperature is increased, as shown in Figure 30. The BET surface area of Cs or Ba promoted catalysts remain about 200-220m^2/g after 4h hydrogen reduction at 350°C (Table 7). In contrast, the surface area drops to 120-150m^2/g if hydrogen treatment is performed at 400°C. While loss of surface area may explain the drop in activity of the catalyst after heat treatment, it may also be due to a sintering of Ru metal particles because of the structural loss of the support and

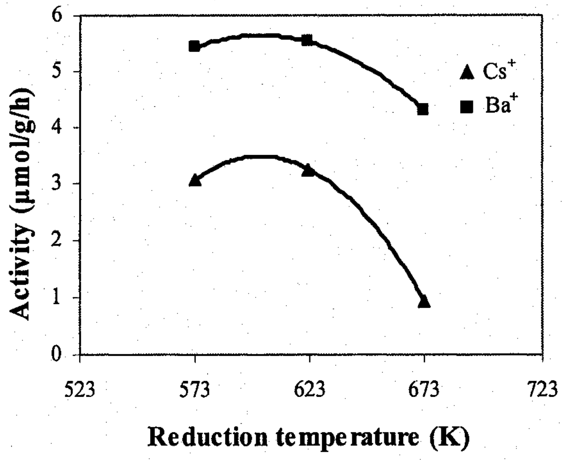

Figure 30. Activity of ammonia synthesis on 5 wt% Ru-Cs/Ta and Ru-Ba/Ta oxides (promoter/Ru=1 mol/mol) as a function of the reduction temperature. The rate was measured at 623K.

Table 7. Promoter effect on the rate of ammonia synthesis over 5 wt% Ru/Ta oxide.

Promoter element (M)	Promoter precursor	M/Ru (mole ratio)	BET surface area* (m^2/g)	Activity (μmol/g) over 3h		
				298K	448K	623K
None			319	0.22	0.28	0.55
Cs	$CsNO_3$	1	213	1.44	1.72	6.37
Ba	$Ba(NO_3)_2$	1	220	1.78	4.35	11.56
La	$La(NO_3)_3$	1	208	0	0	8.19

* BET surface areas were measured after catalysts were activated by H_2 at 623K for 4h, and catalytic run at 623K for 3h.

increased diffusion of Ru particles at higher temperatures, although we could not confirm this by XRD. Conversely, the loss of activity may be related to a migration of promoter oxides from the Ru metal surface or an evaporation of promoter oxides from the catalyst, as has been observed previously. [67] The decrease in activity at higher temperature is more extensive for the $CsNO_3$ promoted catalyst than the $Ba(NO_3)_2$ promoted analogue, possibly because the former metal oxide tends to vaporize more easily than the latter metal oxide at high temperature. Although catalysts with lower H_2 reduction temperature at 300°C have somewhat higher surface areas at the range of 240-260m^2/g, the lower activities are more likely related to lower decomposition percentage of the promoter precursors. Figure 31 shows the H_2-TDA results of $Ba(NO_3)_2$ promoted Ru catalysts.

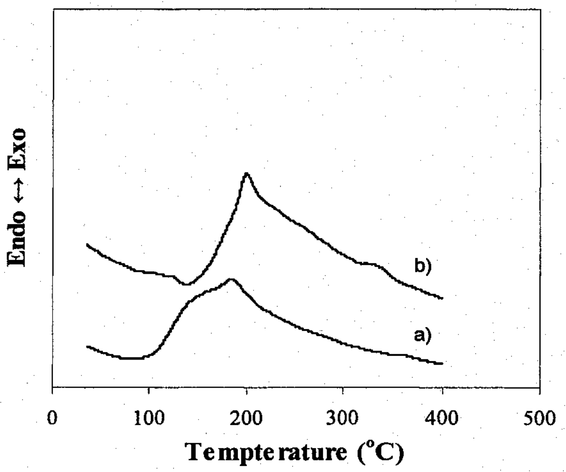

Figure 31. H_2-DTA of Ru/Ta oxide catalysts promoted with $Ba(NO_3)_2$ for (a) Ba/Ru=1, and (b) Ba/Ru=3.

There is a strong exothermal peak between 190-250°C that can be attributed to the reduction of promoter precursors and liberation of gaseous nitrogen species from surface nitrate. The reduction of nitrate in the presence of Ru has been shown to occur between

200 °C and 250 °C. [71, 106] A higher promoter/Ru molar ratio moves the exothermal towards higher reduction temperature with a stronger peak. No exothermal peak was observed below 450°C in the absence of Ru, which provides further evidence for the role of Ru particles in the reduction of nitrate during the activation process. In previous studies it was found that much of the initial high activity of the catalysts occurred only if this pre-reduction step was not conducted and the entire catalytic run performed in the presence of both N_2 and H_2. Thus, if the catalyst is first reduced in H_2 and then a catalytic run started, the activities are thus generally much lower. Since nitrate reduction in the presence of H_2 generally proceeds through an N_2 intermediate, the degradation of active sites is likely a major contributor to this lower activity. Preliminary kinetic data also suggest that the rate of ammonia production depends more strongly on H_2 concentration than N_2 concentration. These and other kinetic effects are currently under investigation to arrive at a more detailed picture of the nature of the active site and the detailed reaction mechanism. Since this paper is focusing on compositional effects rather than mechanistic studies, this is out of the scope of this work.

4.2.3 Effect of Different Promoters

Although the most widely accepted mechanism for ammonia synthesis over Ru-based catalysts is one in which electron density from the promoter is first donated to the Ru metal grains and then transferred to the dinitrogen antibonding orbital to weaken the robust N-N triple bond, this is still a matter of contention as the detailed role of the promoter has never fully elucidated. [75] Some disagreements have arisen from conflicting experimental observations, however these may be attributed to some extent to the different support materials used and promoters used in the various catalytic systems in question. [67, 72, 73] Previous studies by a number of groups have shown that alkali metal Cs and alkali earth metal Ba promoters are the two best choices for Ru-based Haber systems. The supports employed in these studies include active carbon (A.C.), oxides (MgO, Al_2O_3), zeolite (X, Y) and MCM41 mesoporous silica. One anomaly is that rare earth metal La promoters are the most effective for Al_2O_3 systems. This has been explained by a SMSI (strong-metal support interaction) effect, which is related to coverage by the promoter of the precious metal surface when this surface is reduced to a lower valency.[107] For the sake of completeness, all three of these promoters were selected and tested in our Ru-doped mesoporous Ta oxide catalyst system. The activities of these catalysts are compared in Table 7. These results clearly show that Ba is the best promoter for our Ru/Ta oxide system. $La(NO_3)_3$ promoted catalysts didn't show any activity in our system below 250°C, but are active above this threshold. This could be attributed to the SMSI effect of La, as observed in the alumina systems.

Rationalizing why the Ba promoter should work best in a system that clearly may involve a different mechanism than the standard Haber catalysts (in so far as the variable oxidation states of the Ta oxide support may be involved) requires some knowledge of the role of the support in the traditional systems. It is generally accepted that the presence of a K promoter in Fe based Haber systems not only greatly enhances the reactivity of previously inactive Fe surfaces (e.g. Fe(110), Fe(210)), but also lowers the energy of adsorption of ammonia on the Fe metal.[60] Therefore, as the concentration of NH_3 on the surface decreases, more active sites remain available for dissociative adsorption of N_2. Studies on thermal desorption spectroscopy of NH_3 by Benndorf and Madey suggested a similar mechanism for catalysis on Na-doped Ru (001).[108] Aika and co-workers have proposed that rate enhancement by alkali or alkali earth metal promoters in Ru-based systems result from electronic promotion. Electron density is donated from the promoter to the Ru, lowering its ionization potential, which allows the electrons at the Ru surface to be readily donated into the N_2 antibonding orbital, thus reducing the activation energy for dissociative adsorption of N_2. [109] Relating this observation to our system, it stands to reason that the effectiveness of electron transfer from Ru to Ta should rely in part on the potential at the surface of the Ru particles. Thus decreasing the binding energy of electrons at the Ru surface should lead to a more effective transfer of electrons to the Ta centers in the generation of low-valent sites, as long as a suitable electron pathway exists between the Ru and the Ta. This would mean that promoters which decrease the binding energy of Ru surface electrons would be more effective in generating reduced Ta sites than those promoters which increase the binding energy of surface electrons, and would lead to an increase in the reaction rate if, indeed, reduced Ta is involved in the nitrogen cleavage step.

The role of the Ba in our system may not be so simple, however, as various other groups have done studies that suggest that electron density is not transferred from alkali promoters to the Ru metal, [110] and the electrostatic interaction is limited to the vicinity of the alkali [111] or that efficient electron transfer occurs to oxygen rather than ruthenium. [112] This is supported by the observation that the addition of promoters to the catalytic systems in question generally does not cause a significant change in the activation energies. However when $Ba(NO_3)_2$ is used as promoter for Ru/MgO catalyst, a large decrease in apparent activation energy for ammonia production is observed. [75] But this unusual change is apparently not due entirely to the effect of Ba since this drop in activation energy doesn't occur in the Ba-Ru/zeolite X system; the apparent activation energy of Ba-Ru/zeolite X catalyst is actually similar to the values for alkali-exchanged zeolite X. Therefore, the combined interaction of promoter, the support, and the Ru metal is possibly responsible for the change in activation energy. Also, according to Aika's mechanism, Ba should never be superior to Cs as an electronic promoter. However, Ba functions as a better promoter than Cs in almost all studied Ru catalyst systems. There are several reasons that have been proposed to explain these surprising experimental results:

1) Similar electronegativities between BaO and CsOH. The promoters typically exist as oxides or hydroxides under reaction conditions. Usually, Ba is considered in the form of oxide (BaO) and Cs in the form of oxide or hydroxide (Cs_2O/CsOH). The values of electronegativities of these compounds are as follows: 1.20 (Cs_2O), 1.73 (CsOH), 1.77(BaO). If Cs^+ works as CsOH just as on Al_2O_3, then the value 1.73 is near to 1.77 of Ba oxide. [67]

2) Promoter ions could be blocking active sites. Barium ion has oxide state of +2, and Cs ion of +1, only half as much as Ba^{2+} as Cs^+ is required for charge balance of the acidic metal oxide framework. [113]

3) Less mobility of BaO than Cs_2O/CsOH. BaO is believed to stay longer than Cs_2O and CsOH on the Ru surface, and contact time between these species is an important factor.

4) Specific surface interaction between support and promoter can play an important role and modify the activity of the promoter depending on the support.

With all of these factors potentially at play and evidence for involvement of low valent Ta in the process, it is not yet possible to delineate the exact reason why Ba functions as the best promoter in our system. The simplest explanation is that it facilitates electron transfer between the Ru and the Ta by modifying the Fermi level of the Ru, but this neglects possible direct interactions between Ba and Ta, or Ba and O, or other factors mentioned above. Clearly more experimental work needs to be done on both the mechanism and structure of the active site before more definite conclusions can be drawn.

4.2.4 Effect of promoter/Ru ratio

Since $Ba(NO_3)_2$ was found to be the best promoter in our system, the amount of $Ba(NO_3)_2$ was systematically varied and the activity was measured. The results are shown in Figure 32. In the case of 5 wt% Ru/Ta oxide catalyst, a Ba/Ru ratio of 1:1 gave the maximum activity at lower temperature, while 3:1 proved the best at higher temperature. The surface of activated mesoporous Ta oxide, with the BET surface area of 242m^2/g, can accommodate 7.13 mmolg^{-1} Ba^{2+} ions or 7.07 mmolg^{-1} Ru when Ba^{2+} ions or Ru are closely packed on the surface.[106] The surface quantities of Ba^{2+} and Ru with promoter/Ru=1 and 5.0 wt % Ru loading are about 0.4 mmolg^{-1} and 0.4 mmolg^{-1} respectively, and cover only about 5.6% and 5.7% of surface of Ta oxide, respectively.

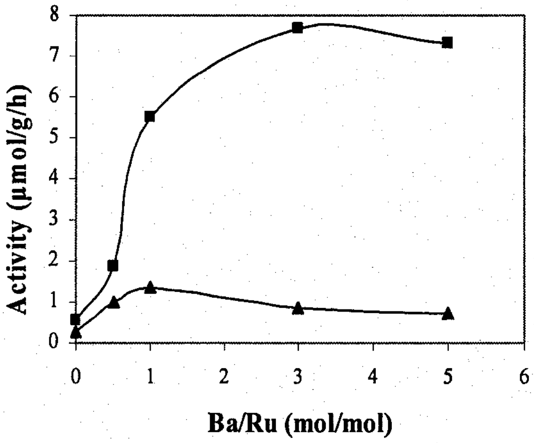

Figure 32. Activity of ammonia synthesis on 5 wt% Ba-Ru/Ta as a function of Ba/Ru mol ratio. ▲: rate was measured at 448Kon the catalyst reduced at 623K; ■: rate was measured at 623K on the catalyst reduced at 623K.

According to Aika's mechanism, in the case of an acidic support like Ta oxide, a small amount of an alkaline promoter will be consumed to neutralize the support and so a higher promoter/Ru is preferred. Jacobsen and co-workers, by using atomic-resolution in situ TEM observed that Ba atoms distributed as single atoms close to the crystal edges (B_5 sites) and bound to oxygen are responsible for the electronic promotion of the catalyst. [114] Since very few such active sites are present in the catalyst, it appears that the majority of Ba atoms from relatively large, optimal Ba/Ru ratio (0.3~2.0) [115-117] are used as reservoirs to maintain a constant coverage of mobile Ba atoms in the vicinity of all B_5-type sites in the catalyst.

While Ru is the active agent for the standard Haber process at high temperature, with all bond breaking and forming processes occurring on the metal surface, XPS results show that reduced Ta sites on the support are be involved in our system. The activity of the catalyst at elevated temperature shows a strong dependence on the Ru/Ba ratio and a maximum activity at 3:1, which is similar to traditional Haber catalysts. However, the plot at lower temperature shows far less of a dramatic dependence on this ratio and a maximum at 1:1. It is thus conceivable that two mechanisms may be at work in varying proportions depending on temperature. At higher temperature the majority of ammonia is generated at the Ru surface, while at lower temperature where traditional Haber catalysts are generally inactive, the second mechanism involving reduced Ta predominates. Another explanation is that because of the much higher molecular weight of Ta_2O_5 than other supports, only 4.5mmol Ta atoms present in 1 gram of Ta oxide. Excessive promoter could thus block the active Ta sites and for this reason a somewhat lower ratio is preferable at lower temperature. Catalysts with an even higher ratio of 5:1 were also tested at 350°C and relatively low activity was found. In this case XPS studies showed that only about 85% $Ba(NO_3)_2$ was decomposed to BaO under our activation conditions.

4.2.5 Effect of Absolute Ru Loading

Ru /Ta oxides prepared from $Ru_3(CO)_{12}$ using different Ru loading were prepared and doped with $Ba(NO_3)_2$ at a Ba/Ru ratio of 1. The rates of ammonia synthesis from these catalysts at 448 K and 623 K are shown in Figure 33. The rate increases linearly with Ru loading at 623 K, but increases only slightly before leveling off at 448 K. This pattern of greater dependency on dopant levels at higher temperature is consistent with the results from Figure 32. Aika and co-workers have observed a linear relationship up to 5 wt% of Ru loading over their Ru/MgO systems, [73] which is not unexpected since with the entire catalytic reactions take place on the Ru clusters in these systems. However, in our Ru/Ta oxide catalysts, the Ru could also function as an interface to funnel electrons from H_2 to the Ta reducible sites at lower temperature. The fact that activity does not increase with Ru loading at 448 K is in accord with a new mechanism, at least at this temperature, in

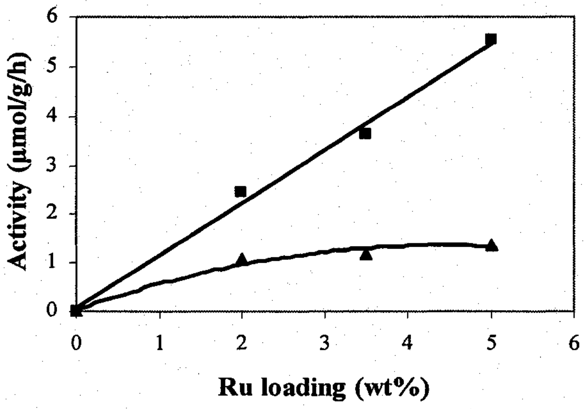

Figure 33. Activity of ammonia synthesis at 448K (▲) and 623K(■) as a function of Ru loading.

which the number of reduced Ta active sites might be more important than Ru and the rate of reaction depends more strongly on electron transfer between the Ru and the Ta. This is in accord with the low activation energies measured previously, which suggest a small number of very active sites. Once the electrons are transferred to the Ta, the reaction proceeds rapidly, consistent with the almost instantaneous cleavage of N_2 and subsequent formation of NH_3 in bis(toluene) Ti reduced mesoporous Ta oxide. Thus, the limiting factor is transfer of electrons to the Ta and the low activities coupled with low activation barrier can be explained by the presence of only limited effective electron transfer pathways in the material. Increasing the temperature does not improve electron transport, but allows the second mechanism to become more important. This hypothesis also suggests that improving electron transport across the surface should lead to more reduced Ta sites and higher activities and is supported by the fact that Ba is the best promoter and is known to influence the energy of the electrons at the Ru surface and thus their facility for mobility across the surface.

4.2.6 Effect of Ba and Ru precursor

Promoter precursor effects of $Ba(OH)_2$ and Ba(isopropoxide) were examined and compared with that of $Ba(NO_3)_2$ using . The activities were measured in each case after hydrogen reduction was complete and all ammonia formed during this initial period (arising from nitrate or residual N_2 in the system) ruled out. The results of this study are shown in Table 8. All the Ba salts are effective, with $Ba(NO_3)_2$ giving the best results at both 448 K and 623 K. $RuCl_3.3H_2O$ was also used as an alternative of Ru precursor. These catalysts were prepared by impregnating $RuCl_3.3H_2O$ with mesoporous Ta oxide in methanol, and further promoted by $Ba(OH)_2$ and Ba(isopropoxide). The activities of thus prepared catalysts were compared with that of the standard catalyst and the results also shown in Table 8. The trend follows exactly that using $Ru_3(CO)_{12}$ as the precursor. A possible explanation for the observation that $Ba(OH)_2$ is a poorer promoter than $Ba(NO_3)_2$ may be due to the lower basicity of BaO originating from the hydroxide rather than $Ba(NO_3)_2$. The reason that Ba isopropoxide didn't exert a promotion effect may be because it didn't decompose completely to BaO under our operating conditions. From Table 8 it can also be seen that $RuCl_3.3H_2O$ is not as good precursor as $Ru_3(CO)_{12}$. This is not surprising based on results from standard Haber systems and has been related to three major effects. Ru exists as Ru^{3+} in the parent catalyst, which has to be reduced before nitrate promoters decompose. $Ba(NO_3)_2$ is not reduced with H_2 below 450°C in the absence of Ru. On the other hand, because of the nature of the precursor and the method of decomposition used, there is already some Ru metal existing in parent $Ru_3(CO)_{12}$ catalyst before H_2 treatment, so that Ru-catalyzed nitrate decomposition in this case should be more facile. Another major reason that $RuCl_3.3H_2O$ is a less effective precursor is that chloride ions are known to poison the catalyst. Aika and co-workers found that much higher activities can be obtained after removal of chloride at very higher temperatures, for example 1000°C. [118] Magnesia was also found to be one of the best oxide supports for ammonia synthesis, especially when $Ru_3(CO)_{12}$ was used as precursor.

Table 8. Effect of Ru and Ba precursor

Ru precursor compound (5 wt %)	Ba precursor compound	Ba/Ru (mole ratio)	BET surface area* (m^2/g)	Activity (μmol/g/h)	
				448K	623K
$Ru_3(CO)_{12}$	$Ba(NO_3)_2$	1	220	1.38	5.52
	$Ba(OH)_2$	1	252	0.42	0.75
	$Ba[OCH(CH_3)_2]_2$	1	232	0	0.13
$RuCl_3.xH_2O$	$Ba(NO_3)_2$	1	225	0.34	1.87
	$Ba(OH)_2$	1	249	0.16	0.51
	$Ba[OCH(CH_3)_2]_2$	1	241	0	0.08

* BET surface areas were measured after catalysts were activated by H_2 at 623K for 4h (barium nitrate precursor), or 2h (other barium precursors), followed by catalytic run at 623K for 3h.

[73] The high activities might be contributed from high Ru dispersion, the chloride-free system and the basicity of MgO. Finally, water vapor from $RuCl_3.3H_2O$ could also be another poison and thus decrease the catalyst activity when used as a source of Ru. [71]

4.3 Conclusion

For the mesoporous Ta oxide catalytic system, $Ru_3(CO)_{12}$ and $Ba(NO_3)_2$ were found to be the most effective precursors of Ru catalysts. $La(NO_3)_3$ showed a poorer promoter at mild conditions but a better promoter at high enough temperature than $CsNO_3$ probably due to the SMSI effect. Studies on Ru/Ba ratio and absolute Ru loading show different behaviors at 448 K and 623 K, suggesting that two mechanisms may be at play, one related to the standard Haber process, and a second consistent with the proposal made previously on the basis of Arrhenius data and XPS that a different mechanism might be functioning due to the involvement of Ta species with variable oxidation states. However, the longevity for ammonia synthesis over this catalyst is less than that over other Ru-based catalysts. This may be due in part to the gradual loss of meso-structure during the various processing such as wet impregnation and prolonged heating; however other factors may also be at play. Further mechanistic investigations of this new catalytic system are ongoing with an effort to better understand the controlling factors and thus be able to develop strategies to improve activity and longevity.

Chapter 5. Conclusion

The exploration of mesoporous materials as catalysts or catalyst supports has been an area of much interest since the first M41S series of mesoporous silicates were synthesized in 1992. In spite of the great amount of work done in this area, there is only one report of MCM-41 used in Haber ammonia synthesis. This is surprising since nitrogen activation remains one of the biggest challenges in modern catalysis. In this thesis, I have, for the first time, synthesized variety of mesoporous Ta oxide based catalysts and systematically explored their reactivity for nitrogen activation in terms of Schrauzer's and Haber-Bosch's processes. This electroactive support provides a reaction scaffolding which allows photocatalytic conversion of water and dinitrogen to ammonia, as well as a seemingly new reaction pathway for Haber synthesis, which functions at a lower temperature than the traditional catalysts and uses low valent Ta as an intermediate in the process.

Pure mesoporous Ta oxide is able to photocatalytically convert N_2 and H_2O to NH_3 at a rate of about 0.3μmol/g/h under UV light. This rate is relatively lower when compared with Ti oxide as Schrauzer-type catalyst, and is believed to be the result of an amorphous wall structure or disconnected nanocrystalline grains embedded in the walls, which leads to poor electron-hole separation and a reduction in catalytic efficiency. Heat treatment and suitable Fe^{3+} doping indeed increase the activity to about 0.8μmol/g/h, which is probably attributed to an increase of crystallization and formation of permanent space charge region in the wall thus improve the electron-hole separation. An attempt to further improve electron-hole separation on the surface of the Ta oxide mesostructure by treatment with bis(toluene) titanium has little effect on the activity, probably because the O_2 by-product degrades the very air sensitive surface coat, although an increase of conductivity from this surface coating can be expected.

Ru-based thermal catalysis was also conducted using dihydrogen and dinitrogen. The capacity for variable oxidation states of the support and the high surface area and porosity is particularly intriguing. In fact, the goal of this work was to develop a catalytic process in which the Ta oxide support was active in the mechanism, thus exploiting the well-known propensity for low-valent early transition metals to activate dinitrogen, in particular work by Fryzuk [57]on Ta-based dinitrogen cleavage.

From previous work it was established that a Haber catalyst requires a precious metal, usually Fe or Ru, on a main group oxide support (i.e. magnesia, alumina, silica), as well as a promoter (usually a group I or II metal oxide), the role of which is to tune the reactivity of the active sites. From our studies on Ru-doped mesoporous Ta oxide, BaO appears to be the best promoter. Although this is not unexpected on the basis of previous work, the mechanism in our work and that of others has not yet been fully elucidated. Some related factors established previously include good basicity (although is not as good as Cs_2O), divalent ion charge, strong binding to Ru metal and/or Ta active sites, and special interaction with Ru metal and/or support. For the active metal, $Ru_3(CO)_{12}$ is better precursor in our system than $RuCl_3.3H_2O$, likely because Cl^- and H_2O in the latter precursor are thought to poison the catalyst and decrease the activity. Increased Ru loading clearly improved the activities of catalysts at higher temperature (e.g. 350°C) but didn't change the low-temperature activities very much, suggesting reduced Ta specie(s) rather than Ru metal dominates the activity at low temperature.

Aika and co-workers proposed a mechanism in which Ru metal is the sole active agent for NH_3 synthesis in their Al_2O_3 and MgO systems, and the promoter modifies the surface energy of the Ru electrons at the Fermi level through some form of electron donation, and the electrons at the Ru Fermi level are then donated into N_2 anti-bonding orbital. This electron donation thus enhances the rate-determine N_2 chemisorption step. Interestingly, the reaction order in H_2 is negative, a factor attributed to surface competition and excess chemisorbed H_2 blocking surface sites for N_2 binding. In our Ru-doped mesoporous Ta oxide catalytic system, this mechanism is clearly not operative. Much lower activation energy (Ea=9.3kJ/mol) and very high initial rates, as well as XPS evidence for low valent Ta involvement, suggest that our catalyst has a small concentration of but very active sites. [60] The active sites are believed to consist mostly of Ta specie(s), at least at low temperatures, because

(a) This phenomenon is much similar to the observation of nitrogen cleavage by previously studied bis(toluene) Ti reduced Ti/Ta systems.

(b) XPS provides evidence that different Ta specie(s) are involved in the catalytic reaction and that activity appears related to a small number of sites at very low Ta binding energy.

(c) Linear increase of Ru loading has little effect on activity at low temperatures.

Therefore, we proposed a new mechanism for our mesoporous Ta oxide catalytic systems, in which the Ru acts as an interface to transfer electron density from hydrogen to neighboring Ta sites on the oxide support, which in their reduced form are then able to cleave dinitrogen. This mechanism is consistent with previous findings in our group as well as work by Fryzuk.

In spite of the ability to activate nitrogen at mild conditions, our Ru/Ta catalysts show relatively low activities at higher temperatures (i.e.300°C-400°C) than those previously studied systems such as Ru/MgO, Ru/Al_2O_3 and Ru/MCM41. Except the above mentioned high molecular weight of Ta oxide, three other reasons might be considered:

1) Bulk Ta oxide as well as most supported Ta oxide (e.g. on Al_2O_3, TiO_2, ZrO_2) itself possess only acidic sites; [113, 119] and basic sites are required for effective ammonia synthesis.

2) Ru-based catalyst is somewhat structure sensitive (Fe-based catalyst is highly structure sensitive). Previous studies showed that an optimum size around 2.0nm is necessary to exhibit the highest number of active B_5-type sites primarily located at crystal edges and corners; [120] in our system, Ru particles seem distributed so finely on the surface of mesoporous materials, that even XRD and TEM couldn't resolve the size of Ru clusters.

3) Doping method has great impact on the distribution of metal particles within the pore structure as well as the stability of mesostructure. When wet impregnation is necessary, water as a solvent should be avoided to the greatest extent because it destroys the pore structure due to capillary forces.

4) Because of the very active and sensitive properties of our catalysts, higher purity of synthesis gases is desirable to avoid the quick deactivation of the catalysts.

Future work

New directions in our group following the exciting discoveries reported in this thesis include detailed kinetic studies and labeling studies to probe into the role of nitrate in the initial and highly active first hour. In particular, crossover isotope studies with ^{15}N labeled N_2 and barium nitrate will be carried out in order to prove whether the nitrate reduction goes through an N_2 intermediate. Varying concentrations of N_2 and H_2 will also help establish the mechanism of this reaction and whether the ammonia in the first hour and that produced after nitrate decomposition is being formed by the same mechanism. Other precious metal dopants will also be tried as well as other support materials such as mesoporous Nb oxide, in an effort to improve the activities. If the rate depends on surface conductivity of electrons from the precious metal to the active group V metal, then obtaining a match between the Fermi levels of the two phases will be required for an Ohmic contact allowing unhindered electron transfer.

While vanadium oxides (bulk mixed metal oxides and supported metal oxides) have seen a lot of applications in catalysis [121-123] because of the existence of combined redox sites and acidic sites, niobium oxides, possessing primary (Lewis) acidic characteristics, have also received much attention in recent years [124-127] when used as additives or supports. However, the current knowledge of the physical and chemical properties of tantala-based catalytic materials is rather limited.

Because of its high dielectric constant, Ta oxide is used as optical coating or in electronics technology as capacitor material; [128, 129] hydrated tantalum oxide is highly acidic, and alumina-, zirconia-, and titania- supported tantalum oxide shows dominant Lewis acidity, as well as Brønsted acidity at higher Ta coverage due to the presence of Ta-OH. Interestingly, silica-supported tantalum oxide gives rise to a considerable redox activity as well at higher Ta loading as the interaction between tantala and silica occurs; [119] Similar to niobium oxide, tantalum oxide easily reacts with many other oxides to form mixed metal oxide phases with complex structure, and remarkably enhance catalytic activity and selectivity and prolong catalyst life. Finally, the promotion effects of Ta and

Nb oxide on environmental catalysts, namely catalysts for the pollution abatement, have aroused much attention.[130]

Supported tantalum oxides can be physically characterized by XRD, UV-Vis DRS, IR, Raman[119] and XANES/EXAFS[131] spectroscopy to determine the nature of the surface species, and chemically probed by the N_2 physical adsorption and various chemisorption probe molecules (e.g. pyridine, CH_3OH[132]), as well as H_2-TPR(hydrogen temperature programmed reduction) and CH_3OH oxidation reaction.[132, 133] However, there is no spectroscopic method available to directly describe the outer surface of bulk metal oxide catalytic systems.[132]

Mesoporous materials fall into a size range between molecular and bulk, and therefore show unusual physical properties that are not observed in either state. Extensive studies are necessary to explore the physical, electronic and reactivity properties of mesoporous Ta oxide and related catalytic systems. For this concern, ^{17}O appears to be a good probe to the local structure. Work in our group with M. E. Smith in England is being conducted in order to delineate the microstructure of the walls by this technique.

With excellent acidic property, as well as controlled pore size (20-50Å) and high surface area (400-900m^2/g), mesoporous Ta oxide (also Nb oxide) is promising for solid acid catalyst and catalyst support in a wide range of important petrochemical reactions. A project to investigate the catalytic properties of mesoporous Ta and Nb oxides for isomerization of alkanes and alkylation of benzene with olefins is ongoing. The potential of coupling hydrocarbon skeletal rearrangements with nitrogen activation is intriguing from the standpoint of nitrogen incorporation into fine organics. It appears that mesoporous Ta oxides require an electron source and an electrophile source (H^+ in this thesis) to activate N_2. Using a hydrocarbon as the electron source and a carbocation generated on the surface as the electrophile may indeed lead to interesting reactivity.

The exploration of mesoporous Ta oxide as the first catalyst support with variable oxidation states has thus already led to new reactivity not seen in traditional systems and promises to exhibit a rich and diverse chemistry in the future.

References

(1) Berzelius, J. *Jahres-Bericht über die Fortschritte der Physichen Wissenschaften*, Volume 15, H. Laupp, Tübingen, **1836**.

(2) Laidler, K. J. *The World of Physical Chemistry*, Oxford University Press, Oxford, **1993**.

(3) Taylor, H. S. *J. Am. Chem. Soc.* **1931**, 53, 578.

(4) Thomas, J. M.; Thomas, W. J. *Introduction to the Principles of Heterogeneous Catalysis*, Academic Press, London, **1967**.

(5) *Chem. Ind.*, 21 January **2002**, P. 22.

(6) Thomas, J. M.; Thomas, W. J. *Principles and Practice of Heterogeneous Catalysis*, VCH, Weinheim, **1996**.

(7) Rabo, J. A.; Risch, A. P.; Poutsma, M. L. *J. Catal.* **1978**, 53, 295.

(8) Kasšpar, J.; Fornasiero, P.; Hichey, N. *Catal. Today*, **2003**, 77, 419.

(9) Barteau, M. A.; Madix, R. J. *The Chemical Physics of Solid Surface and Heterogeneous Catalysis*, Elsevier Pub. Co., **1982**.

(10) Rao, V. N. M. *Proceedings of the 8th North American Meeting of the Catalysis Soc.*, Paper D-23, **1983**.

(11) Tauster, S. J.; Fung, S. C.; Garten, R. J. *J. Am. Chem. Soc.* **1978**, 100,170.

(12) Stone, F. S. *J. Solid State Chem.* **1975**, 17, 271.

(13) Marcilly, Ch.; Delmon, B. *J. Catal.* **1972**, 24, 336.

(14) Sleight, A. W. *Advanced Materials in Catalysis*, Academic Press, New York, **1977**.

(15) Keulks, G. W. *J. Catal.* **1970**, 19, 232.

(16) Hagg, W.O.; Lago, R. M; Weisz, P. B. *Nature*, **1984**, 309, 589.

(17) Meisel, S. L.; McCullough, J. P.; Lechthaler, C. H.; Weisz, P. B. *Chem. Technol.*, **1976**, 6, 86.

(18) Topsoe, H.; Clausen, B. S.; Candia, R.; Wivel, C.; Morup, S. *Bull. Soc. Chim. Belg.*, **1981**, 90, 1189.

(19) Behrens, P.; Stucky, G. D. *Angew. Chem. Int. Ed. Engl.* **1993**, 32, 696.

(20) Kresge, C. T.; Leonowicz, M. E.; Roth, W. J.; Vartuli, J. C.; Beck, J. S. *Nature* **1992**, 359, 710.

(21) Beck, J. S.; Vartuli, J. C.; Roth, W. J.; Leonowicz, M. E.; Kresge, C. T.; Schmitt, K. D.; Chu, C. T.-W.; Olson, D. H.; Sheppard, E. W.; McCullen, S. B.; Higgins, J. B.; Schlenker, J. L. *J. Am. Chem. Soc.* **1992**, 114, 10834.

(22) Vartuli, J. C.; Schmitt, K. D.; Kresge, C. T.; Roth, W. J.; Leonowicz, M. E.; McCullen, S. B.; Hellring, S. D.; Beck, J. S.; Schlenker, J. L.; Olson, D. H.; Sheppard, E. W. *Chem. Mater.* **1994**, 6, 2317.

(23) Huo, Q.; Margolese, D. I.; Ciesla, U.; Feng, P.; Gier, T. E.; Sieger, P.; Leon, R.; Petroff, P. M.; Schüth, F.; Stucky, G. D. *Nature* **1994**, 368, 317.

(24) Huo, Q.; Margolese, D. I.; Ciesla, U.; Demuth, D. G.; Feng, P.; Gier, T. E.; Sieger, P.; Firouzi, A.; Chmelka, B. F.; Schüth, F.; Stucky, G. D. *Chem. Mater.* **1994**, 6, 1176.

(25) Monnier, A.; Schüth, F.; Huo, Q.; Kumar, D.; Margolese, D.; Maxwell, R. S.; Stucky, G. D.; Krishnamurty, M.; Petroff, P.; Firouzi, A.; Janicke, M.; Chmelka, B. F. *Science* **1993**, 261, 1299.

(26) Firouzi, A.; Atef, F.; Oertli, A. G.; Stucky, G. D.; Chmelka, B. F. *J. Am. Chem. Soc.* **1997**, 119, 3596.

(27) Tanev, P. T.; Pinnavaia, T. J. *Science* **1995**, 267, 865.

(28) Bagshaw, S. A.; Prouzet, E.; Pinnavaia, T. J. *Science* **1995**, 269, 1242.

(29) Bagshaw, S. A.; Pinnavaia, T. J. *Angew. Chem. Int. Ed. Engl.* **1996**, 35, 1102.

(30) Antonelli, D. M.; Ying, J. Y. *Curr. Op. Colloid Interface Sci.* **1996**, 1, 523.

(31) Antonelli, D. M.; Nakahira, A.; Ying, J. Y. *Inorg. Chem.* **1996**, 35, 3126.

(32) Antonelli, D. M.; Ying, J. Y. *Angew. Chem. Int. Ed. Engl.* **1996**, 35, 426.

(33) Antonelli, D. M.; Ying, J. Y. *Chem. Mater.* **1996**, 8, 874.

(34) Wong, M. S.; Ying, J. Y. *Chem. Mater.* **1998**, 10, 2067.

(35) Yang, P.; Zhao, D.; Margolese, D. I.; Chmelka, B. F.; Stucky, G. D. *Nature* **1998**, 396, 152.

(36) Yang, P.; Zhao, D.; Margolese, D. I.; Chmelka, B. F.; Stucky, G. D. *Chem. Mater.* **1999**, 11, 2813.

(37) Ciesla, U.; Demuth, D.; Leon, R.; Petroff, P.; Stucky, G.; Unger, K.; Schüth, F. *J. Chem. Soc., Chem. Commun.* **1994**, 1387.

(38) Sayari, A. *Chem. Mater.* **1996**, 8, 1840.

(39) Yusuf, M. M.; Imai, H.; Hirashima, H. *J. Sol-gel Sci. and Tech.* **2002**, 25, 65.

(40) Takahara, Y.; Kondo, J. N.; Takata, T.; Lu, D.; Domen, K. *Chem. Mater.* **2001**, 13, 1194.

(41) Stone Jr., V. F.; Davis, R. *J. Chem. Mater.* **1998**, 10, 1468.

(42) Perkas, N.; Wang, Y.; Koltypin, Y.; G edanken, A.; Chandrasekaran, S. *Chem. Commun.* **2001**, 11, 988.

(43) Yoshitake, H.; Tatsumi, T. *Chem. Mater.* **2003**, 15, 1695.

(44) Carreon, M. A.; Guliants, V. V.; Pierelli, F.; Cavani, F. *Catal. Lett.* **2004**, 92, 1-2, 11.

(45) Hidai, M.; Mizobe, Y. *Chem. Rev.* **1995**, 95, 1115.

(46) Kim, J.; Rees, D. C. *Nature* **1992**, 360, 553.

(47) Howard, J.B.; Rees, D. C. *Chem. Rev.* **1996**, 96, 2965.

(48) Einsle, O.; Tezcan, F. A.; Andrade, S. L. A.; Schmid, B.; Yoshida, M.; Howard, J. B.; Rees, D. C. *Science* **2002**, 297, 1696.

(49) Leigh, G.J. *Acc. Chem. Res.* **1992**, 25, 177.

(50) Laplaza, C. E.; Cummins, C. C. *Science* **1995**, 268, 861.

(51) Nugent, W.A.; Mayer, J. M. *Metal-Ligand Multiple Bonds*, Wiley, New York, **1988**.

(52) Fryzuk, M. D.; Love, Jason B.; Rettig, Steven J.; Young, Victor G. *Science* **1997**, 275, 1445.

(53) Fruzuk, M. D.; Johnson, S. A. *Coord. Chem. Rev.* **2000**, 200-202, 379.

(54) Yandulov, D. V.; Schrock, R. R. *Science,* **2003**, 301, 76.

(55) Pool, J. A.; Lobkovsky, E.; Chirlk, P. J. *Nature*, **2004**, 427, 527.

(56) Fomitchev, D. V.; Bagley, K. A.; Coppens, P. *J. Am. Chem. Soc.* **2000**,122, 532.

(57) Fryzuk, M. D.; Johnson, S. A.; Patrick, B. O.; Albinati, A.; Mason, S. A.; Koetzle, T. F. *J. Am. Chem. Soc.* **2001**,123, 3960.

(58) Ertl, G. *Critical Reviews in Solid State and Materials Science*, CRC Press, Boca Raton, FL, **1982**, Volume 10, P. 349.

(59) Strongin, D. R.; Carrazza, J.; Bare, S. R.; Somorjai, G. A. *J. Catal.* **1987**, 103, 213.

(60) Somorjai, Gabor A. *Introduction to Surface Chemistry and Catalysis*, A Wiley-Interscience Publication, **1994**.

(61) Jacobsen, C. J. H. *Chem. Commun.* **2000**, 1057.

(62) Report article: *Appl. Catal.* **1991**, 67, N18.

(63) Aika, K.; Hori, H.; Ozaki, A. *J. Catal.* **1972**, 27, 424.

(64) Hinrichsen, O. *Catal. Today* **1999**, 53, 177.

(65) Kika, K.; Kumasaka, M.; Oma, T.; Kato, O.; Matsuda, H.; Watanabe, N.; Yamazak, K.; Ozaki, A.; Onishi, T. *Appl. Catal.* **1986**, 28, 57.

(66) Bécue, T.; Davis, R. J.; Garcest, J. M. *J. Catal.* **1998**, 179, 129.

(67) Aika, K.; Kawahara, T.; Murata, S.; Onishi, T. *Bull. Chem. Soc. Jpn.*, **1990**, 63, 1221.

(68) Goethel, P. J.;Yang, R. T. *J. Catal.* **1988**, 111, 220.

(69) Baker, R. T. K. *Carbon* **1986**, 24, 715.

(70) Cisneros, M. D.; Lunsford, J. H. *J. Catal.* **1993**, 141, 191.

(71) Aika, K.; Shimazaki, K.; Hattori,Y.; Ohya, A.; Ohshima, S.; Shirota, K.; Ozaki, A. *J. Catal.* **1985**, 92, 296.

(72) Murata, S.; Aika, K. *J. Catal.* **1992**, 136, 110.

(73) Aika, K.; Takano, T.; Murata, S. *J. Catal.* **1992**, 136, 126.

(74) Murata, S.; Kika, K. *J. Catal.* **1992**, 136, 118.

(75) Fishel, C. T.; Davis, R. J.; Garces, J. M. *J. Catal.* **1996**, 163, 148.

(76) Vettraino, M.; He, X.; Trudeau, M.; Drake, J. E.; Antonelli, D. M. *Adv. Funct. Mater.* **2002**, 3, 174.

(77) Vettraino, M.; Trudeau, M.; Lo, A. Y. H.; Schurko, R. W.; Antonelli, D. M. *J. Am, Chem. Soc.* **2002**, 124, 9567.

(78) Lezau, A.; Skadtchenko, B.; Trudeau, M.; Antonelli, D. M. *J. Chem. Soc. Dalton Trans.* **2003**, 4115.

(79) Davis, R. J.; Gainer, J.; O'Neal, G.; Wu, I.-W. *Water Environ. Res.* **1994**, 66, 50.

(80) Al-sayyed, G.; D'Oliveira, J. C.; Pichat, P. *J. Photochem. Photobiol. A* **1991**, 58, 99.

(81) Saladin, F.; Forss, L.; Kamber, I. *J. Chem. Soc. Chem. Commun.* **1995**, 533.

(82) Yamagata, S.; Nishijo, M.; Murao, N.; Ohta, S.; Mizoguchi, I. *Zeolites* **1995**, 15, 490.

(83) Bard, A. J.; Fox, M. A. *Acc. Chem. Res.* **1995**, 28, 141.

(84) Sayama, K.; Tanaka, A.; Domen, K.; Maruya, K.; Onishi, T. *J. Catal.* **1990**, 124, 541.

(85) Tanaka, K.; Harada, K.; Murata, S. *Sol. Energy* **1986**, 36, 159.

(86) Schrauzer, G. N.; Guth, T. D. *J. Am. Chem. Soc.* **1977**, 99, 7189.

(87) Palmisano, L.; Augugliaro, V.; Sclafani, A.; Schiavello, M. *J. Phys. Chem.* **1988**, 92, 6710.

(88) Hoshino, K. *Chem. Eur. J.* **2001**, 7, 2727.

(89) Bazhenova, T. A.; Shilov, A. E. *Coord. Chem. Rev.* **1995**, 144, 69.

(90) Wang, Y.; Tang, X.; Lin, L.; Huang, W.; Hacohen, Y. R.; Gedanken, A. *Adv. Mater.* **2000**, 12, 1183.

(91) Mamak, M.; Coombs, N.;, Ozin, G. *Adv. Mater.* **2000**, 12, 198.

(92) Rosowski, F.; Hornung, A.; Hinrichson, O.; Herein, D.; Muhler, M.; Ertl, G. *Appl. Catal.* **1997**, 151, 443.

(93) Ye, B.; Trudeau, M.; Antonelli, D. M. *Adv. Mater.* **2001**, 13, 561.

(94) Ye, B.; Trudeau, M.; Antonelli, D. M. *Chem. Mater.* **2002**, 14(6), 2774.

(95) He, X.; Trudeau, M.; Antonelli, D. M. *Adv. Mater.* **2000**, 12, 1036.

(96) He, X.; Antonelli, D. M. *Angew. Chem. Int. Ed. Engl.* **2002**, 41, 214.

(97) Murray, S.; Trudeau, M.; Antonelli, D. M. *Adv. Mater.* **2000**, 12, 1339.

(98) Vettraino, M.; Trudeau, M.; Antonelli, D. M. *Adv. Mater.* **2000**, 12, 337.

(99) Yue, C.; Trudeau, M.; Antonelli, D. M. *Can. J. Chem.* **2005,** 83, 308.

(100) Bielawa, H.; Hinrichsen, O.; Birkner, A.; Muhler, M. *Angew. Chem. Int. Ed.* **2001,** 40, 1061.

(101) Strongin, D. R.; Somorjari, G. A. *J. Catal.* **1988**, 109, 51.

(102) Ueda, A.; Haruta, M. *Gold Bulletin* **1999**, *32*(1), 3.

(103) Skadtchenko, B. O.; Trudeau, M.; Schurko, R. W.; Lo, A. Y. H.; Antonelli, D. M. *Chem. Mater.* **2005**, 17, 1467.

(104) Schlögl, R. *Angew. Chem. Int. Ed.* **2003,** 42, 2004.

(105) Yue, C.; Trudeau, M.; Antonelli, D. M. *Angew. Chem. Int. Ed.* Submitted.

(106) Liang, C.; Wei, Z.; Luo, M.; Ying, P.; Xin, Q; Li, C. *Studies in surface science and catalysis* **2001**, 138, 283.

(107) Tauster, S. T.; *Acc. Chem. Res.* **1987**, 20, 389.

(108) Benndorf, C.; Madey, T. E. *Chem. Phys. Lett.* **1983**, 101, 59.

(109) Aika, K.; Ohya, A.; Ozaki, A.; Inoue, Y.; Yasmuri, I. *J. Catal.* **1985**, 92, 305.

(110) Uner, D. O.; Pruski, M.; Gerstein, B. C.; King, T. S. *J. Catal.* **1994**, 114, 530.

(111) Lang, N. D.; Holloway, S.; Nørskov, J. K. *Surf. Sci.* **1985**, 150, 24.

(112) Over, H.; Bludau, H.; Skottke-Klein, M.; Moritz,W.; Ertl,G. *Phys. Rev. B* **1992**, 46, 360.

(113) Wachs, I. E.; Chen, Y.; Jehng, J.-M.; Briand, L. E.; Tanaka, T. *Catal. Today* **2003**, 78, 13.

(114) Hansen, T. W.; Wagner, J. B.; Hansen, P. L.; Dahl, S.; Topsøe, H.; Jacobsen, C. J. H. *Science* **2001**, 294, 1508.

(115) Kowalczyk, Z.; Jodzis, S.; Raróg, W.; Zielinski, J.; Pielaszek, J.; Presz, A. *Appl. Catal. A* **1999**, 184, 95.

(116) Formi, L.; Molinari, D.; Rossetti, I.; Pernicone, N. *Appl. Catal. A* **1999**, 185, 269

(117) Bielawa, H.; Hinrichsen, O.; Birkner, A.; Muhler, M. *Angew. Chem.* **2001**, 113, 1093.

(118) Murata, S.; Aika, K. *Appl. Catal.* **1992**, 82, 1.

(119) Baltes, M.; Kytokivi, A.; Wechhuysen, B. M.; Schoonheydt, R. A.; Voort, P. V.D.; Vansant, E. F. *J. Phys. Chem. B* **2001**, 105, 6211.

(120) Jacobsen, C. J. H.; Dahl, S.; Hansen, P. L.; Törnqvist, E.; Jensen, L.; Topsøe, H.; Prip, D. V.; Møenshaug, P. B.; Chorkendorff, I. *J. Mol. Catal. A.* **2000**, 163, 19.

(121) Bond, G. C.; Vedrine, J. C.; *Catal. Today* **1994**, 20 (1) (special issue).

(122) Vedrine, J. C.; *Catal. Today* **2000**, 56 (4) (special issue).

(123) Trifiro, F.; Grzybowska, B. *Appl. Catal. A* **1997**, 157 (special issue).

(124) Ko, E. I. *Catal. Today* **1990**, 8 (1) (special issue).

(125) Tanabe, K. *Catal. Today* **1993**, 16 (3–4) (special issue).

(126) Tanabe, K. *Catal. Today* **1996**, 28 (1–2) (special issue).

(127) Schmal, M.; Silva,V. T. d.; Noronha, F.B. *Catal. Today* **2000**, 57 (3–4).

(128) Meng, J. F.; Rai, B. K.; Katiyar, R. S.; Halla, A. S. *J. Phys. Chem. Solids* **1997**, 58, 1530.

(129) Pollard, K. D.; Puddephatt, R. J. *Chem. Mater.* **1999**, 11, 1069.

(130) Ushikubo, T. *Catal. Today* **2000**, 57, 331.

(131) Tanaka, T.; Nojima, H.; Yamamoto, T.; Takenaka, S.; Tunabiki, T.; Yoshida, S. *Phys. Chem. Chem. Phys.* **1999**, 1, 5235.

(132) Briand, L. E.; Farneth, W. E.; Wachs, I. E. *Catal. Today*, **2000**, 62, 219.

(133) Tatibouët, J. M *Appl. Catal. A* **1997**,148, 213.

Vita Auctoris

Name: Chaoyang Yue

Place of Birth: Jiangxi, China

Education: Wuhan University of Technology, China

1985-1989 Honor B. Eng.

University of Windsor, Canada

2002-2005 M. Sc.

Publications:

(1) Yue, C.; Trudeau, M.; Antonelli, D. M. *Can. J. Chem.* **2005,** 83, 308.

(2) Yue, C.; Trudeau, M.; Antonelli, D. M. *Angew. Chem. Int. Ed.* Submitted.